

FABRICATION AND CHARACTERIZATION OF BIOFERROELECTRIC COMPOSITES

By

Amarilis Declet-Vega

A thesis submitted in partial fulfillment of the requirements for the degree of

MASTER OF SCIENCES
IN
MECHANICAL ENGINEERING
UNIVERSITY OF PUERTO RICO
MAYAGUEZ CAMPUS
2015

Approved by:

O. Marcelo Suárez, Ph.D.
President, Graduate Committee

Date

Pedro Quintero, Ph.D.
Member, Graduate Committee

Date

Ricky Valentín, Ph.D.
Member, Graduate Committee

Date

Ricky Valentín, Ph.D.
Chair, Mechanical Engineering Department

Date

Edgardo Lorenzo, Ph.D.
Representative of Graduate Studies

Date

ABSTRACT

Bio-ferroelectric composites have recently sparked intensive research in order to develop inexpensive and environmental electronic devices such as capacitors, transistors, and actuators. The present research involves the synthesis of composites made of a chitosan-cellulose polymeric layer and ferroelectric nanoparticles. To fabricate the bio-ferroelectric composites, a chitosan/cellulose layer was synthesized followed by a layer containing ferroelectric nanoparticles. The variables considered includes the volume percentage of cellulose (15v% and 25v%) in the matrix and the amount of ferroelectric nanoparticles (10wt% and 20wt%). Additionally, the acetic acid concentration upon synthesis was studied due to its effects on the swelling degree of the composites. The composites underwent tensile, thermogravimetric and thermomechanical tests. Furthermore, dielectric properties were measured; including capacitance, dielectric constant, current density, and electrical resistivity. In order to analyze their sustainability for electronic applications, the composites were degraded under different acid solutions. The results showed that higher percentages of cellulose decreased the ultimate tensile strength (UTS) and the degradation temperature T_{deg} of the chitosan-cellulose composites while the addition of cellulose slightly raised the UTS and T_{deg} of the chitosan-cellulose composites with strontium titanate nanoparticles. Conversely, our results demonstrated that the acidity of the solution decreased the mentioned mechanical and thermal properties. The most interesting part consisted in the study of the dielectric properties; capacitors with higher dielectric constants were fabricated. Additionally, our capacitors are able to withstand higher voltages; the dielectric breakdown of the bioferroelectric composites at 60V was not observed.

RESUMEN

Recientemente, los compuestos bio-ferroeléctricos son investigados para desarrollar nuevos componentes eléctricos tales como: capacitores, transistores y actuadores. En esta investigación se fabricaron compuestos de quitosano-celulosa con partículas ferroeléctricas. Para la fabricación de los compuestos bio-ferroeléctricos se sintetizó una película de quitosano-celulosa seguido por una película polimérica con partículas ferroeléctricas. Entre las variables consideradas se encuentran: el porcentaje por volumen de celulosa (15p/v y 25p/v) y el porcentaje por peso de nanopartículas ferroeléctricas (10p/p y 20 p/p). Además, se consideró la concentración de ácido acético (1.25 p/v y 2.50 p/v) debido a su efecto directo en la retención de agua en el polímero. A estos bio-compuestos se les realizaron pruebas de tensión, termomecánicas y termales. También se analizaron las propiedades eléctricas de los compuestos tales como: capacitancia, constante dieléctrica, flujo de corriente a través del capacitor y resistividad eléctrica. Altos porcentajes de celulosa disminuyeron la máxima resistencia mecánica y la temperatura de degradación de los compuestos de quitosano-celulosa. Sin embargo, la adición de celulosa aumentó las propiedades mecánicas y termales de los compuestos con nanopartículas ferroeléctricas. Por otra parte, altas concentraciones de ácido acético disminuyeron la resistencia mecánica y la temperatura de degradación de los compuestos. La parte más interesante de nuestra investigación consistió en el estudio de las propiedades dieléctricas del material; se logró fabricar exitosamente capacitores con altas constantes dieléctricas a bajas frecuencias. Estos capacitores lograron resistir 60V y no se observó una ruptura dieléctrica del capacitor.

Copyright © 2015
Amarilis Declet Vega
All rights reserved

ACKNOWLEDGEMENTS

Thanks to God for His blessings through my life. Special thanks to my family; Francisco J. Marrero, Luis A. Declet, Esther Vega and Luis J. Declet for their patience, comprehension, continuous support and love.

I would like to express my sincere appreciation to my advisor, O. Marcelo Suárez, for giving me the opportunity to work in his research group from 2010-2015. Thanks for his guidance, and valuable advises in the academic, professional and personal life.

Also, I would also like to thank to my friends: Boris Renteria, Carlos Rivera, Ulises Barajas, Sujeily Soto, David Florían, Nitza García, Marta Rozo, Armando Peña and Gina Montes for giving me the support through my research. Thanks' to my undergraduate students: Nelson Sepúlveda, Javier Martínez and Edgardo Reyes for their invaluable work and cooperation thought the research.

I which to thank the National Science Foundation for its support under Grant HRD 0833112 (CREST program): Nanotechnology Center for Biomedical and Energy-Driven Systems and Applications and the Department of General Engineering for its financial support.

TABLE OF CONTENTS

ABSTRACT	ii
RESUMEN	iii
ACKNOWLEDGEMENTS	v
LIST OF FIGURES.....	viii
LIST OF TABLES.....	xi
ACRONYMS AND ABBREVIATIONS	xii
1 INTRODUCTION	1
1.1 Literature Review	2
1.1.1 Synthesis of Chitosan-Cellulose Films and Fibers.....	2
1.1.2 Polymer-ferroelectric Composites.....	5
1.2 Research Objectives	11
2 THEORETICAL BACKGROUND	13
2.1 Biopolymers	13
2.2 Ferroelectric Ceramics	16
2.3 Polarization	18
2.4 Polarization Mechanisms	19
2.5 Dielectric Properties	21
2.5.1 Dielectric Constant	22
2.5.2 Dielectric Strength	24
2.5.3 Resistivity	24
2.6 Thermomechanical Analysis	26
2.6.1 Glass Transition Temperature (T_g)	26
2.6.2 Creep Analysis	27
3 EXPERIMENTAL PROCEDURE	32
3.1 Materials Selection.....	32
3.2 Fabrication of Chitosan-Cellulose Polymeric Films	32
3.3 Fabrication of Bio-Ferroelectric Composites	34
3.4 Materials Characterization.....	37
3.4.1 Structure Analysis.....	37
3.4.2 Mechanical Analysis	37
3.4.3 Thermal Analysis	38
3.4.4 Electrical Analysis.....	39

4	CHARACTERIZATION OF CHITOSAN-CELLULOSE BIO-COMPOSITES	41
4.1	Thermogravimetric Analysis (TGA)	41
4.2	Tensile Analysis	43
5	CHACTERIZATION OF BIO-FERROELECTRIC NANOCOMPOSITES.....	46
5.1	SrTiO ₃ Nanoparticles.....	46
5.2	Thermogravimetric Analysis (TGA)	49
5.3	Tensile Tests.....	50
5.3.1	Thermomechanical Analysis.....	51
5.4	Electrical Properties	62
5.4.1	Capacitance and Dielectric Constant Measurements	63
5.4.2	Current Density and Resistivity Measurements	65
5.4.3	Electrical Measurements of Chitosan-Cellulose-STO nanoparticles and Commercial Ceramic Capacitors.....	67
5.5	Degradation Analysis	69
6	CONCLUSIONS	78
7	REFERENCES	82

LIST OF FIGURES

Figure 1. Dielectric constant for chitosan-blended cellulose composites [12].....	6
Figure 2. Dielectric constant as a function of the electric field for nanocomposites made of chitosan and barium titanate nanoparticles [13].	7
Figure 3. Dielectric constant measurements at different percentages of barium titanate nanoparticles in the composite: (1) 0%, (2) 2%, (3) 10% and (4) 33% [14].	8
Figure 4. Polarization mechanisms	19
Figure 5. Schematic of a capacitor which consists of a dielectric material and parallel plates on both sides of the dielectric material.....	23
Figure 6. Crystalline and amorphous phases in a semi-crystalline polymer.	26
Figure 7. Strain of a polymer as a function of the temperature.....	27
Figure 8. (a) Spring element and (b) dashpot element.	28
Figure 9. (a) Maxwell model and (b) Kelvin model.	29
Figure 10. Sequence of the fabrication of chitosan-cellulose films.....	34
Figure 11. Experimental procedure of the fabrication of chitosan-cellulose films with ferroelectric nanoparticles.	36
Figure 12. Calframo™ stirrer clamp utilized in the measurement of the dielectric properties.	40
Figure 13. TGA analysis for bio-composites made of 1.5 v% chitosan / (0.5 v% and 1.0 v%) cellulose and 1.25 v% of acetic acid.	Error! Bookmark not defined.
Figure 14. TGA analysis for bio-composites made of 1.5v% chitosan / 0.5v% cellulose considering 1.25v% and 2.50v% of acetic acid.	43
Figure 15. Tensile analysis for bio-composites made of 1.5 v% chitosan / (0.5 v% and 1.0 v%) cellulose and 1.25 v% of acetic acid.	44
Figure 16. Tensile analysis for bio-composites made of 1.5 v% chitosan / 0.5 v% cellulose considering 1.25 v% and 2.50 v% of acetic acid.	45
Figure 17. XRD pattern of STO powder after 10 hours of milling.	47
Figure 18. STO particle size as a function of milling time.....	48

Figure 19. Scanning electron microscopy images obtained from a bio-ferroelectric nanocomposite (20 wt% STO): (a) low magnification; (b) high magnification.....	48
Figure 20. TGA analysis for bio-composites made of 1.5 v% chitosan / 0.5 v% cellulose considering 20 wt%, 10 wt% and 0 wt% of strontium titanate nanoparticles.	49
Figure 21. Tensile analysis for bio-composites made of 1.5 v% chitosan / 0.5 v% cellulose considering 20 wt%, 10 wt% and 0 wt% of STO nanoparticles.	50
Figure 22. Glass transition temperature (T_g) for biopolymers made of 5 v%, 15 v% and 25 v% of cellulose.	52
Figure 23. Glass transition temperature (T_g) for bio-composites made of 15 v% and 25 v% of cellulose and 10 wt% STO nanoparticles.	53
Figure 24. Glass transition temperature (T_g) for bio-composites made of 15 v% and 25 v% of cellulose and 20 wt% STO nanoparticles.	53
Figure 25. Creep strain as a function of time for a nanocomposite made of 15 v% of cellulose and 0 wt% STO nanoparticles.	55
Figure 26. Creep strain as a function of time for a nanocomposite made of 15 v% of cellulose and 20 wt% STO nanoparticles.	55
Figure 27. Schematic structure of nanoparticles-semicrystalline polymer composites. .	56
Figure 28. Creep rate as a function of time for a nanocomposite made of 15 v% of cellulose and 0 wt% STO nanoparticles.	58
Figure 29. Creep rate as a function of time for a nanocomposite made of 15 v% of cellulose and 20 wt% STO nanoparticles.	58
Figure 30. Creep compliance as a function of time for a nanocomposite made of 15 v% of cellulose and 0 wt% STO nanoparticles.	59
Figure 31. Creep compliance as a function of time for a nanocomposite made of 15 v% of cellulose and 20 wt% STO nanoparticles.	59
Figure 32. Viscosity study of bio-composites made of 15 v% Cel containing 0 wt% STO and 20 wt% STO nanoparticles.	61
Figure 33. Capacitance as a function of frequency at an electric field of 1V.	63
Figure 34. Dielectric constants as a function of frequency at an electric field of 1V.	64

Figure 35. Current density as a function of voltage for bio-ferroelectric nanocomposites.	66
Figure 36. Resistivity as a function of cellulose percent of the bio-ferroelectric nanocomposites.	67
Figure 37. Capacitance measurements for the polymer / STO nanocomposite and four commercial ceramic-disk capacitors.....	68
Figure 38. Current flow at different voltages: (a) commercial capacitors and experimental one; (b) detail of the polymer-STO nanocomposite response.....	69
Figure 39. Absorbed mass as a function of time for bio-composites made of chitosan, cellulose and STO nanoparticles degraded in hydrochloric acid solution, pH 3.3.	70
Figure 40. Absorbed mass as a function of time for bio-composites made of chitosan, cellulose and STO nanoparticles degraded in acetic acid solution, pH 4.1.	70
Figure 41. Absorbed mass as a function of time for bio-composites made of chitosan, cellulose and STO nanoparticles degraded in water, pH 6.0.....	71
Figure 42. Polymer chains under different pH values: (a) pH 7.0; (b) pH 4.0 [49].	72
Figure 43. Dry mass for bio-composites made of chitosan, cellulose and STO nanoparticles.....	73
Figure 44. Dissolution rate constant (k_{dis}) for bio-composites made of chitosan, cellulose and STO nanoparticles.....	74
Figure 45. Fourier transform infrared spectra for bio-composites made of 25 v% of cellulose in acetic acid solution.	75
Figure 46. Fourier transform infrared spectra for bio-composites made of 25 v% of cellulose in hydrochloric acid solution.	75
Figure 47. Tensile analysis for degraded bio-composites made of 15 v% and 25 v% of cellulose in hydrochloric acid solution.	76
Figure 48. Tensile analysis for degraded bio-composites made of 15 v% and 25 v% of cellulose in hydrochloric acid solution.	76

LIST OF TABLES

Table 1. Tensile strength and swelling of chitosan-cellulose composites from unreduced or reduced cellulose [7].	3
Table 2. Tensile strength obtained from dry and wet films [8].	4
Table 3. Dielectric constant of PVDF and PMMA at different temperatures [13].	9
Table 4. Dielectric constant of PVDF with barium strontium titanate and strontium titanate nanoparticles [13].	10
Table 5. Electrical properties of titanates.	21
Table 6. Burger coefficients for biocomposites made of 0 wt% STO nanoparticles.	60
Table 7. Burger coefficients for bio-composites made of 20 wt% STO nanoparticles. ..	60

ACRONYMS AND ABBREVIATIONS

Some terms were abbreviated to explain process or characterization in the research. The following list provides the expansion of the abbreviated terms:

Chitosan polymer	Ch
Cellulose polymer	Cel
Strontium titanate nanoparticles	STO
Acetic acid solution	Ac
Degradation temperature	T_{deg}
Glass transition temperature	T_g
Ultimate tensile strength	UTS
Creep compliance	$J(t)$
Current density	J
Resistivity divided by the thickness	ρ_t
Thickness of the sample	t
Dissolution rate constant	k_{dis}
X-ray diffraction	XRD
Thermogravimetric analysis	TGA
Thermomechanical analysis	TMA
Fourier transform infrared spectroscopy	FTIR

1 INTRODUCTION

Biopolymers have attained great potential in the market due to their vast applications in diverse fields: “bio-ceramic, bio-sensing, biomedical engineering, bio-nanotechnology and biologically assembly” [1]. Recent and increasing interest in these materials is due to their unique characteristics such as: biocompatibility, eco-friendly qualities, and nontoxicity [2], [3]. Furthermore, these polymers can be recycled or can require a low cost treatment to do so. As a result, the fabrication process is less extensive and more cost effective, as opposed to man-made synthetic polymers. Some biopolymers currently studied are chitosan and cellulose that are obviously environmentally friendly. At this point, it is deemed important to underscore that biopolymers can effectively interact with non-organic elements to create new composites. One relevant example is the formulation of a ferroelectric/biopolymer composite, which possesses unique properties that arise from joining a plastic organic compound with a hard ceramic one.

Nowadays, ferroelectric particles trigger interest as an alternative for processable high permittivity materials [4], [5]. Appealing properties of these particles include high dielectric constant, moderate dielectric strength, high specific electrical resistivity, low dielectric loss, among others [4], [5]. These characteristics made these materials suitable for the fabrication of capacitors, transistors, actuators, etc. As mentioned, the ferroelectric nanoparticles are incorporated into polymers seeking for specific electrical properties of the composite. In the last decades, scientists and researchers fabricated nanocomposites in which the organic matrix is a bio-polymer. As a result, new studies aim at the fabrication of new composites bearing a biopolymer as the organic matrix. The ferroelectric materials can be employed in high dielectric constant capacitors, medical diagnostic transducers,

electro-optic light valves, radio and communication filters, and positive temperature coefficients [6].

The present research involves the development of a composite made of a chitosan-cellulose matrix reinforced with ferroelectric nanoparticles. The intended addition of cellulose enhances the flexibility of the bio-ferroelectric nanocomposites due to the brittle behavior of chitosan. In addition, the ferroelectric nanoparticles are incorporated to functionalize the composite and make it suitable for diverse electronic applications.

1.1 Literature Review

As mentioned, chitosan and cellulose are the most studied biopolymers due to their unique characteristics such as biocompatibility, biodegradability and non-toxicity. Additionally, the fabrication process is unsophisticated and cost effective, which makes it attractive for researchers who are focused into developing new composites made of a polymeric matrix and nanoparticles. The present thesis details the fabrication and characterization of a novel nanocomposite made of chitosan-cellulose and ferroelectric nanoparticles for improved electrical properties.

1.1.1 Synthesis of Chitosan-Cellulose Films and Fibers

Natural polymers as matrices of composites have sparked the interest of scientists and researchers. For instance, Hosokawa and Nordqvist fabricated bio-composites made of chitosan and cellulose. Hosokawa et al. studied the mechanical properties of the composites, which were related to the crosslinking effect between chitosan and cellulose [7]. They discovered that the carbonyl (C=O) and carboxyl groups (C–OH) in the cellulose structure affect the crosslinking and its formation depend on the oxidation-reduction

method applied to the cellulose polymer. The oxidation-reduction method increased the presence of these functional groups in the cellulose structure. To fabricate the chitosan-cellulose films, a stock solution of chitosan and cellulose was prepared. The chitosan polymer was dissolved in water and acetic acid, whereas the cellulose fibers were diluted in an aqueous solution after oxidation and reduction. A small amount of chitosan was added into the cellulose solution containing glycerol. The resulting solution was mechanically stirred and degassed before being placed on a polystyrene dish to dry.

Hosokawa analyzed the chemical structure of chitosan-cellulose composites by Fourier transform infrared spectroscopy (FTIR). The absorbance registered at 1590 cm^{-1} corroborated the presence of amine groups, corresponding to the primary functional groups of chitosan. Furthermore, the absorbance at 1370 cm^{-1} indicates the presence of the C–H groups pertaining to the cellulose structure.

In addition, Hosokawa and collaborators measured the resulting tensile strength and swelling, as shown in Table 1. Dry films with unreduced cellulose exhibited higher strength and lower swelling. The authors suggested that the presence of carbonyl groups in unreduced cellulose affected the wet strength and the swelling of the composites [7].

Table 1. Tensile strength and swelling of chitosan-cellulose composites from unreduced or reduced cellulose [7].

Composites	Tensile Strength kg/cm^2		Swelling
	Dry films	Wet films	
unreduced micro fibril cellulose, carbonyl content = 33.3mmol/kg cellulose	532	365	1.21
reduced micro fibril cellulose, carbonyl content = 5.1mmol/kg cellulose	521	266	1.50

This research also revealed that the swelling depends on the acidity of the solution. In this case, chitosan was dissolved in a water/acetic acid solution, which contributes in the acidity of the solution; the authors demonstrated that a higher swelling correlates with lower pH values.

In another research of interest, Nordqvist et al. fabricated and studied four types of films made of chitosan-cellulose composites: chitosan without microfibrillated cellulose (chitosan A) and chitosan containing microfibrillated cellulose (chitosan AMFC). After obtaining chitosan A and chitosan AMFC, both films were treated with a tris-hydrochloric acid buffer. The buffered films were classified as chitosan B and chitosan BMFC [8].

For the fabrication of chitosan A, the polymer was dissolved in a water/acetic acid solution without adding microfibrillated cellulose. In order to prepare the chitosan-microfibrillated cellulose, small amounts of a cellulose solution were added to a chitosan solution until a proportion of 5wt% of dry microfibril cellulose (MFC) was reached in the final film. The results showed higher tensile strength for buffered films, as shown in Table 2. Additionally, dry films presented higher strength and Young's modulus, while wet films were more likely to be deformable.

Table 2. Tensile strength obtained from dry and wet films [8].

Composites	Tensile Strength (MPa)	
	Dry films	Wet films
Chitosan A	38 ± 5	5 ± 3
Chitosan AMFC	59 ± 9	14 ± 4
Chitosan B	88 ± 16	13 ± 6
Chitosan BMFC	89 ± 14	19 ± 8

As presented, high tensile strength have been observed by Hosokawa and by Nordqvist. Higher values of tensile strength were reported by Hosokawa, who added glycerol into

the composites made of chitosan and cellulose [7]. The addition of glycerol raised the polar groups (–OH), increasing the content of water in the polymeric films. Nemet et al. stated that the polar groups along the glycerol chains reduced the intermolecular forces between the polymers chains [9]. As a result, the molecular spacing and the mobility of the polymer chains increased, retaining the water molecules between the chains. At high pressure and temperature (70°C), large water content is removed from the polymeric matrix, which effects a tensile strength increment. Cheng et al. and Chang et al. demonstrated that by adding glycerol, the polymeric films can withstand high temperature without affecting the structure of the polymers [10], [11]. On the other hand, Nordqvist placed the polymeric films in a tris-hydrochloric acid buffer treatment, which can degrade the films. Additionally, the films were dried at 23°C, a lower temperature to remove the excess of water in the polymeric films.

Of particular interest to this thesis was, in recent years, the addition of ferroelectric nanoparticles for the fabrication of polymer-based nanocomposites. These ferroelectric nanoparticles help adjust the electrical properties of the polymeric matrix, which in general does not possess attractive electrical properties. For this reason, some studies of polymer-ferroelectric composites are rendered in the following section.

1.1.2 Polymer-ferroelectric Composites

Historically, ceramic materials have been employed in ferroelectric composites to improve their dielectric properties. However, recent studies developed novel materials based on organic and ceramic materials in which the organic matrix provides flexibility to the composite.

In one example, Jang et al. studied the electrical properties of chitosan-blended cellulose (CBC) [12]. The solutions were prepared with different chitosan blending levels dissolved in an acid solution: 0 wt% to 40 wt%. Cellulose was treated with de-ionized water, methanol and acetone in order to remove water. Additionally, the cellulose and chitosan were heated at 110°C to remove the remaining water in the polymers. After that, the CBC films were obtained by spin coating, utilizing the chitosan blending solutions. In order to neutralize the free amino groups and produce fixed cations (NH_3^+), the films were treated with NaOH and HCl solutions, and then washed with de-ionized water.

At lower frequency values, the dielectric constant increased, which also was affected by the amount of chitosan blending, as shown in Figure 1. They attributed this to the space charge accumulation and the concentration of ions resulting from the chitosan blending. As mentioned before, the ion mobility was also studied by Jang et al. who discovered that high humidity raised the ion mobility due to the content of water adsorbed by the cellulose, a hydrophilic polymer.

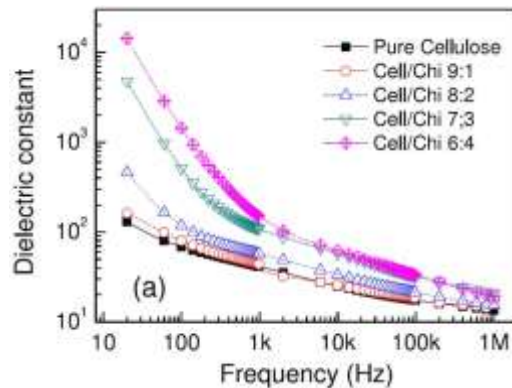


Figure 1. Dielectric constant for chitosan-blended cellulose composites [12].

Furthermore, Neagu et al. focused on the electrical properties of BaTiO_3 -chitosan composites, especially on the dielectric constant with different percentages of BaTiO_3

particles: 0%, 1% and 10% [13]. For the fabrication of the composites, BaTiO₃ powder was prepared by a solid state reaction of BaCO₃ and TiO₂. The BaTiO₃ powder was sieved before being added to the chitosan solution to avoid agglomeration sites in the chitosan matrix. The resulting BaTiO₃ powder was then dispersed in the chitosan solution. In order to improve the BaTiO₃ particles dispersion in the chitosan solution, all the suspensions were magnetically mixed for 4 h. To fabricate the polymeric films, the chitosan/BaTiO₃ solutions underwent a dry phase inversion casting process. The results showed that the addition of BaTiO₃ particles slightly increased the dielectric constant from 42.5 to 47.5, as presented in Figure 2. This research presents a simple approach for generating flexible structures based on polar polymers filled with ferroelectric materials.

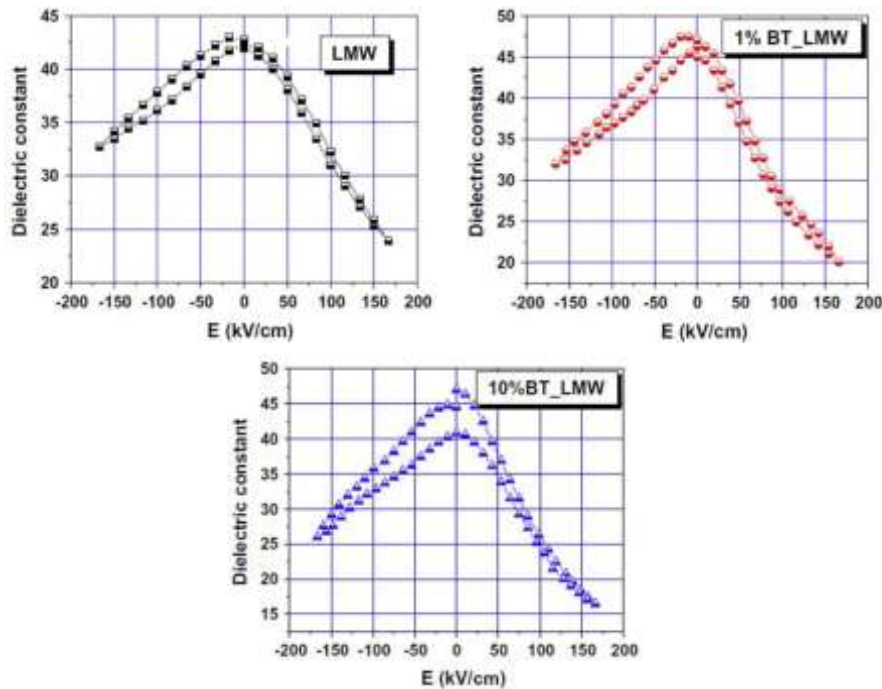


Figure 2. Dielectric constant as a function of the electric field for nanocomposites made of chitosan and barium titanate nanoparticles [13].

The precipitation of barium titanate nanoparticles via plant pathogenic fungus was studied by Bansal and collaborators [14]. A solution of barium acetate and potassium hexafluorotitanate precipitated the nanoparticles in the presence of fungus, which was separated from the solution via filtration. To remove the fungal residues, the nanoparticles were washed and calcined until the protein residues were degraded. The characterization was performed before and after the calcination process. After this calcination process, the particle size increased from 4nm to 8nm.

For dielectric measurements, the titanate nanoparticles were added to poly (methyl methacrylate) (PMMA), and the dielectric properties were measured at room temperature and at frequencies from 1MHz to 1Hz [14]. The amount of nanoparticles varied from 0% to 33%. The results showed that higher percentages of nanoparticles in the composite increased the dielectric constant, which decreased at higher frequencies, as evidenced in Figure 3. For a BaTiO₃-PMMA nanocomposite, the higher dielectric constant achieved was 100, for 33% of nanoparticles.

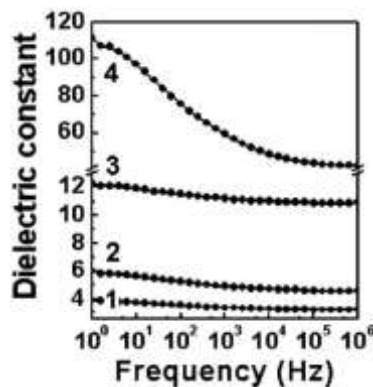


Figure 3. Dielectric constant measurements at different percentages of barium titanate nanoparticles in the composite: (1) 0%, (2) 2%, (3) 10% and (4) 33% [14].

Another study based on composites made of an organic/inorganic matrix was conducted by Gorzkowski et al., who fabricated a ceramic-polymer nanocomposites based on polyvinylidene fluoride (PVDF) and PMMA [15]. In this case, barium strontium titanate (BST) and strontium titanate (ST) nanoparticles were added to the polymeric films. The experimental procedure consisted of dissolving the polymer into the solvent and mixing it with ceramic particles. The solution contained polyhedral oligomeric silsesquiox (POSS) particles to improve the dispersion of the ceramic particles. After casting the solution onto a glass slide, the solution dried in air. Finally, the resulting films were removed for electrical property measurements at room temperature and at 77K (-196.15°C). The author also analyzed the dielectric constant of both polymers without nanoparticles.

The results in Table 3 suggested that higher dielectric constants were acquired for PVDF than for PMMA at room temperature [15]. Also, those results showed that the addition of POSS slightly affected the dielectric constant. Since PVDF possesses high dielectric constant, it was used to analyze the effects of the nanoparticles in the dielectric properties in which the nanoparticles increased the dielectric constant of PVDF, as shown in Table 4. BST nanoparticles at room temperature produced higher dielectric constants than the ST nanoparticles. In the PVDF polymer, the authors discovered that the dielectric constant increased with the amount of ceramic nanoparticles in the nanocomposite.

Table 3. Dielectric constant of PVDF and PMMA at different temperatures [15].

Temperature °C	Dielectric Constant			
	PVDF	PVDF+POSS	PMMA	PMMA+POSS
25	7.8	6.9	3.5	3.5
-196.15	2.7	2.7	2.8	2.8

Table 4. Dielectric constant of PVDF with barium strontium titanate and strontium titanate nanoparticles [15].

Temperature °C	Dielectric Constant		
	PVDF	PVDF+POSS +35v% BST	PVDF+POSS +35v% ST
25	7.8	19.9	14.0
-196.15	2.7	6.2	6.4

This research also uncovered that the addition of BST nanoparticles lowered the dielectric breakdown strength of the nanocomposites. At liquid nitrogen boiling temperature (77K), there are higher values of dielectric breakdown strength than at room temperature. The authors attributed this reduction in the dielectric break-down to two possible causes: a) local electric field concentration, and b) agglomeration of the nanoparticles.

In addition, Gorzkowski et al. analyzed the dielectric constant of the composites at different frequencies and temperatures. At very higher temperatures, the dielectric constant decreased as well for lower temperatures. As stated in another work by Ahmad, temperature alters the intermolecular forces between the crystalline networks of the polymers, affecting the dielectric constant of the composite [16]. At lower temperatures, as the motion of the chains slows down, the orientation of the dipoles is disturbed. However, at too higher temperatures, the dielectric constant also decreased for the strong vibration of the chains. Similarly, the frequency of the electric field changes the dielectric constant because at lower frequencies, the electric dipoles had enough time to align with the electric field but not at high frequencies [16].

In the study of chitosan-cellulose composites, the amount of chitosan raised the dielectric constant of the material. Moreover, in composites made of chitosan-BaTiO₃ particles the dielectric constant raised as the amount of particles increased. Thereupon, the dielectric

properties of PVDF and barium titanate particles or strontium titanate particles were studied and it was discovered that more particles increased the dielectric constant. Even though the electrical properties of polymer/nanofiller composites were analyzed, a polymeric matrix made of chitosan, cellulose and strontium titanate nanoparticles have been not studied. These composites represent a real alternative for electronic applications for their unique characteristics such as: biocompatibility, eco-friendly qualities, and nontoxicity. Although some interesting features of these composites are their less extensive and more cost effective fabrication process, with their dielectric properties being their most appealing characteristics. Thus, we conclude that composites based on chitosan, cellulose and STO nanoparticles represent an alternative to develop bio-capacitors suitable for electronic applications at low frequencies due to their interesting properties: dielectric constant, current density and resistivity.

1.2 Research Objectives

The objective of the present research is to devise and carried out an effective method to synthesize a composite made of chitosan and cellulose and reinforced with ferroelectric nanoparticles intended to adjust the mechanical properties and tune the resulting electrical properties.

Specific Objectives

The research work focuses on the following specific objectives:

Phase I. Bio-composites

- Fabricate chitosan-cellulose films via solution casting method.

- Characterize chitosan-cellulose films and the effects of small amounts of cellulose into the chitosan matrix via:
 - Thermogravimetric analysis (TGA)
 - Tensile test and thermomechanical analysis (TMA)
 - Degradation analysis

Phase II. Bio-ferroelectric Composites

- Synthesize bio-ferroelectric nanocomposites via a layer-by-layer fabrication method.
- Characterize the bio-ferroelectric nanocomposites and the effects of the nanoparticles on the polymeric matrix, using the following characterization techniques:
 - X-ray diffraction (XRD)
 - Scanning electron microscopy (SEM)
 - Thermogravimetric analysis (TGA)
 - Tensile test and thermomechanical analysis (TMA)
 - Measurement of capacitance, dielectric constant, dielectric strength and electrical resistivity.
 - Degradation analysis

2 THEORETICAL BACKGROUND

2.1 Biopolymers

Biopolymers have emerged with great potential in the market due to their vast applications, such as “bio-ceramic, bio-sensing, biomedical engineering, bio-nanotechnology and biologically assembly” [1]. It was aforementioned that these biopolymers present unique characteristics such as biocompatibility, biodegradability and nontoxicity [2], [3]. Since biopolymers are readily produced by Nature, their synthesis is cost effective and not complex. The most common biopolymers studied include chitin, chitosan and cellulose since they all have many applications in the medical, food, water treatment, industrial and agricultural fields. They also possess good biocompatibility with human body tissues and fluids [17].

After cellulose, chitin is considered the most abundant natural polymer. Chitin consists of groups of β -(1,4)N-acetyl glucosamine, which are repeated in the structure of the polymer with multiple hydrogen bonds [3], [18], [19]. The glucosamine position in the structure can change to α (antiparallel), β (parallel) and γ (combined), which indicates the differences in packing and polarities of the chains [18], [19]. Of those structures, α -chitin is the most stable form and can be dissolved in stronger swelling agents such as aliphatic diamines [3], [20]. Additionally, α -chitin has a highly crystalline structure with intra-inter hydrogen bonding, which limits the access of the solvent into the network [18]. Contrary to α -chitin, the more open structure of β -chitin makes it susceptible to swelling; polar molecules (water or alcohol) can penetrate the structure of β -chitin and destroy the hydrogen bonds of the structure [18]. Consequently, N-dimethylacetamide/LiCl is the most common system to dissolve α -chitin for its crystalline structure [20].

Moreover, chitosan is a cationic polysaccharide with a molecular structure made of hydroxyl and amino groups; the structure consists of D-glucosamine and N-acetyl-D-glucosamine [18], [21]. This biopolymer is a derivative of chitin, produced via the alkaline N-deacetylation of that polymer; this process consists of removing the acetate group and replacing it with an amide group in alkaline solutions [2], [20]. Such degree of deacetylation must be at least about 50% to be considered chitosan and to render it soluble in aqueous acidic media [20]. The mechanism of solubility occurs by protonation of the primary -NH_2 group on the C-2 position of the D-glucosamine repeating unit, by which the polysaccharide is converted to a polyelectrolyte in the acidic media [19]. The properties of chitosan depend on the pH, the molecular weight, the distribution of the acetyl groups in the structure, and the degree of de-acetylation [19]. As mentioned above, at low pH, the amide groups are protonated, increasing the solubility of chitosan in dilute aqueous solutions. On the other hand, the amide groups are deprotonated at high pH values, decreasing the solubility of the polymer [20]. Also, advanced functional materials derived from chitosan can be obtained by its chemical modification using the different functional groups already present in the molecule. N-alkylation, N-acylation, N-carboxyalkylation, and polymer grafting have been used for the chemical modification of chitosan [22], [23].

As aforementioned, cellulose is the most abundant biopolymer in the planet, obtained from plant tissue after purification [20], [24]. This linear syndiotactic polymer consists of β -1,4-glycosidic bonds linked with D-glucopyranose units. In the crystalline structure, every monomer is rotated 180° with respect to its neighbors. Additionally, each glucose monomer consists of three hydroxyl groups (-OH) in the C-2, C-3 and C-6 position. The

rotational conformation of the hydroxyl group on C-6 position can alter the hydrogen bonding pattern and the crystallinity structure, affecting the dissolution of the polymer [24]. As in other polymers, some factors affecting the dissolution of cellulose are the length of the polymer chains and, subsequently, the degree of polymerization (DP), which indicates the number of glucose units present in the chain. As the glucose units increase, the number of hydroxyl groups present in the structure also increases. These hydroxyl groups form complex pattern of hydrogen bonds, causing the need of solvents with high hydrogen bonding capacity for the cellulose dissolution. The most common solvents used for the cellulose dissolution include: dimethylacetamide and lithium chloride (DMAc/LiCl), dimethylsulfoxide and tetrabutylammonium (DMSO/TBAF) and N-Methylmorpholine-N-oxide (NMMO). In addition, cellulose can be dissolved in aqueous alkali media such as sodium hydroxide (NaOH/H₂O), sodium hydroxide/urea and sodium hydroxide/poly(ethylene glycol) (NaOH/PEG). Furthermore, acidic media such as trifluoroacetic acid, dichloroacetic acid, formic acid, and sulfuric acid are useful to dissolve it too.

As stated in the previous section, these biopolymers, i.e. chitin, chitosan and cellulose, are compatible with non-organic particles. This presents a further incentive to study the formulation of ferroelectric/biopolymer composites. As a consequence, such composites reinforced with ferroelectric nanoparticles are appealing to be studied due to their tunable dielectric properties.

2.2 Ferroelectric Ceramics

Ferroelectric ceramics have sparked the interest of many researchers for a number of reasons, their piezoelectricity and pyroelectricity being the most appealing features. In piezoelectric materials, an electrical field is produced by an applied mechanical stress. For pyroelectric materials, a temperature gradient generated an electric field. The ferroelectric behavior of these materials is affected by the spontaneous polarization below a characteristic temperature (known as Curie temperature); this means that ferroelectric materials exhibit an electric dipole moment in the absence of an applied electrical field. The electric dipoles in these ceramic structures are aligned as a consequence of their mutual interactions and crystal symmetry as well as the applied local electric field. For ferroelectric materials, polarization increases as a function of that applied field [5], [25], [26]. When the field is removed, the polarization remains at a finite value, known as remnant polarization, as result of the oriented dipoles being unable to return in the original state. In addition, the magnitude of the electric field needs to be lower than the dielectric breakdown of the material. Summarizing, two conditions are needed to classify the ferroelectric materials: a) spontaneous polarization, and b) reorientation of the dipole moments [25]. As it can be inferred, the spontaneous dipole moments are physically tied to the lattices, whereas lattice parameters that can change with an applied force or temperature. Ferroelectric ceramics are divided in four subcategories [25]:

- 1) tungsten-bronze group,
- 2) oxygen octahedral group (perovskite structure),
- 3) pyrochlore group, and
- 4) bismuth group.

Nowadays, perovskite-type titanate ferroelectric ceramics are the most commonly used: BaTiO₃, SrTiO₃, CaTiO₃ and PbTiO₃. In addition, zirconates and other compounds such as LaGaO₃, LaAlO₃ and KNbO₃ have a perovskite structure, but are not extracted from the mineral perovskite. The perovskite structure can be considered as a type of FCC structure in which the central titanium ion (Ti⁺⁴) is coordinated with six oxygen ions (O⁻²), whereas strontium cations (Sr⁺²) are surrounded by four TiO₆ octahedral. These materials have mixed ionic and covalent bonds, which make them suitable for electronic applications.

As mentioned, spontaneous polarization is affected by the lattice constants of the unit cell, which can change with an applied force or temperature. Some perovskites, such as BaTiO₃ and PbTiO₃, present higher spontaneous polarization where the large size of barium and lead ions increases the size of the unit cell. As a result, since the titanium atom is off-centered in the unit cell, it can be located at a higher or lower position in the cell. Consequently, an electric dipole forms in the unit cell [5], [26].

Furthermore, spontaneous polarization is expected below the Curie temperature of the material, where the effect of the thermal energy is negligible [5], [26]. Then, the spontaneous polarization is kept with the electric dipoles aligned. In titanates below the Curie temperature, the octahedral structure changes from cubic to tetragonal and the titanium cation is off-center in the unit cell causing a permanent electric dipole [5], [26].

In the last decades, ferroelectric ceramics have been extensively used in the fabrication of capacitors. These devices require particular characteristics such as energy storage, as well as the ability to filter out noise and to supply power to other components. To establish the effectiveness of the capacitors, specific dielectric properties are measured. Since

spontaneous polarization is key in ferroelectric materials, this property is discussed in the next section.

2.3 Polarization

As indicated before, ferroelectric nanoparticles possess spontaneous polarization, which is the alignment of permanent or induced atomic or molecular dipole moments with an externally applied electrical field [26]. As the field is applied, the charge carriers are displaced in a free space, allowing the redistribution of the charges present in the dielectric material [26]. These electric dipoles generate a dipole moment, which depends on the magnitude and direction of the applied electrical field [5]. The electric dipole moment (equation 1) consists of two opposite electric charges $\pm q$, which are separated by a distance d [5].

$$\mu = q \cdot d \quad (1)$$

When the dielectric material is placed in an electric field, the induced dipoles and any permanent dipoles turn aligned [5]. The polarization of the material is then described by equation 2 [5].

$$P = N \cdot q \cdot d \quad (2)$$

N is the number of dipoles in the dielectric material, q is the charge, and d is the distance between the two opposite electric charges. As presented, dielectric materials can be polarized using an external electrical field. However, there are four possible polarization

mechanisms in a dielectric: electronic, ionic, dipolar, interfacial, schematically shown in Figure 4 and discussed in the next section [5].

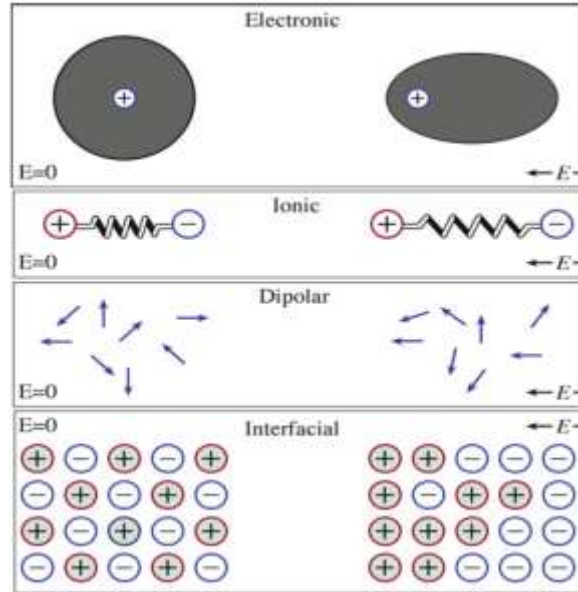


Figure 4. Polarization mechanisms

2.4 Polarization Mechanisms

In the presence of an electrical field, electronic polarization occurs as a result of the displacement of the centered negative electron cloud relative to the positive nucleus of an atom. The electrons concentrate on the side of the nucleus near the positive pole of the electric field. As a result, the atom acts as a temporarily induced dipole. Typical displacements are $\sim 1 \text{ \AA}$, giving a $\mu \sim 1.6 \cdot 10^{-37} \text{ C}\cdot\text{m}$. This is the only possible mechanism in pure materials covalently bonded without permanent dipoles.

Ionic polarization occurs when an electric field is applied to ionically bonded materials. The bonds between the ions are elastically deformed, causing the redistribution of charges, and, thus, increasing the net dipole moment. Additionally, the direction of the

electrical field affects the displacement of the cations and anions that move either closer or farther apart. As a result, as polarization occurs, the dimensions of the unit cell of the material is affected. In this type of polarization, the magnitude of the dipole moment is smaller due to the displacements; 10 to 100 Å are typical displacements.

In dipolar polarization, the substances need to possess a permanent dipole moment. This polarization results from the alignment of the permanent dipole moments onto the direction of the applied electric field. Such alignment is counteracted by the internal energy of the material; this means that thermal vibrations of the atoms decrease the polarization at higher temperatures. In addition, dipolar polarization is generally uncommon in ceramics because most of the permanent dipoles cannot be reoriented without destroying the crystal structure. However, there are some very important exceptions such as perovskite-type ceramics, e.g. barium titanate. In this case, below the Curie temperature, the octahedral coordinated Ti^{4+} ion is displaced and a tetragonal structure is formed, allowing a permanent polarization. When an alternating electric field is applied, the Ti^{4+} ion moves back and forth between the allowable positions to ensure the alignment of the electric dipoles with the electrical field.

In interfacial polarization, when impurities are present, a charge may develop at the interfaces. This charge will move on the surface when the material is placed in an electrical field. The total polarization for the material is cumulative, which means that the total polarization is the sum of all the individual contributions P , as presented in equation 3.

$$P_{\text{total}} = P_{\text{electronic}} + P_{\text{ionic}} + P_{\text{dipolar}} + P_{\text{interfacial}} \quad (3)$$

2.5 Dielectric Properties

Electrical insulators constitute an important field for electronic applications, such as capacitors in electronic circuits and electrical insulators [26]. For these applications, their main properties of interest are the dielectric constant, the dielectric loss factor and the dielectric strength. As electrical insulators, ferroelectric materials bear interesting electrical properties, such as low conductivity or high resistivity, high dielectric constant, moderate dielectric strength, low dielectric loss, among others [27]. In particular, titanates have triggered great interest in industries and researchers due to their appealing electrical properties that are summarized in Table 5 [27]. As mentioned, the most commonly used titanates are: BaTiO₃, SrTiO₃, CaTiO₃ and PbTiO₃.

Table 5. Electrical properties of titanates.

Dielectric Constant 10⁴ Hz	Dielectric Strength V/mm	Volume Resistivity Ohm-cm (23°C)	Loss Factor
15-12,000	50-300	10 ⁸ -10 ¹³	0.0001-0.02

Recent researches have centered on the fabrication of organic materials with ceramic particles because the organic constituent provides additional advantages to the composite, such as cost effectiveness and dimensional accuracy upon fabrication. Additionally, ceramics provide stability upon environmental changes (high temperatures) and thermal stresses. As presented, there are some electrical properties to determine the effectiveness of capacitors: the dielectric constant, dielectric strength and electrical resistivity.

2.5.1 Dielectric Constant

Also known as dielectric constant, the dielectric permittivity is probably the most important property for dielectric materials. The dielectric permittivity (ϵ) relates the electric field with the free charge passing through the surface of the material [26]. This electrical property takes into consideration the capacitance described by equation 4 [26].

$$C = \frac{Q}{V} \quad (4)$$

Q is the charge through the plates and V is the voltage across the capacitor, which stores energy in a given volume.

The capacitance of the material given by equation 4 does not take into account the geometry of the capacitor. As a result, the capacitance for a parallel plate capacitor is given by equation 5 [26].

$$C = \frac{A}{d} \cdot \epsilon \quad (5)$$

A is the area of the plates and d is the distance between the plates. Figure 5 shows a schematic of such capacitor.

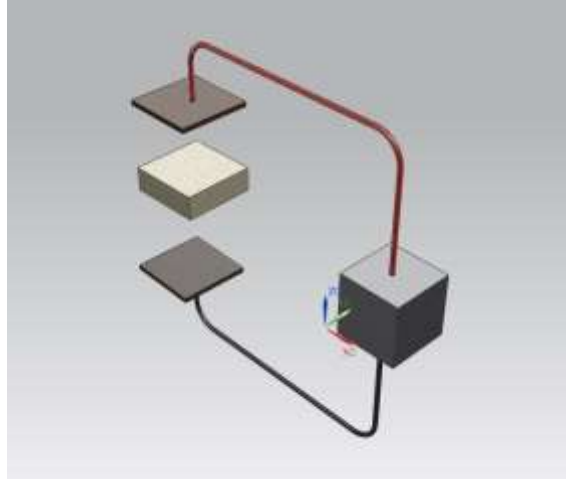


Figure 5. Schematic of a capacitor which consists of a dielectric material and parallel plates on both sides of the dielectric material.

In addition, the dielectric permittivity is given by equation 6 [26].

$$\varepsilon = \varepsilon_0 \cdot k \quad (6)$$

ε_0 is the dielectric permittivity in vacuum and k is the dielectric constant of the material.

The vacuum permittivity value is approximate to $8.854 \times 10^{-12} \frac{F}{m}$ when the plates are attached to the ceramic material and no air flux passes between the plates. After substituting the dielectric permittivity equation into the capacitance equation for a parallel plate capacitor, the dielectric constant is given by equation 7 [26].

$$k = \frac{C \cdot d}{A \cdot \varepsilon_0} \quad (7)$$

C is the capacitance of the dielectric material, A is the area of the plates, d is the distance between the plates and ε_0 , the vacuum permittivity.

2.5.2 Dielectric Strength

The dielectric strength measures the ability of a material to withstand higher electrical fields without breakdown. For a dielectric material, the dielectric strength is given by equation 8 [26].

$$\text{Dielectric Strength} = \frac{V}{t} \quad (8)$$

V is the maximum voltage that withstands the dielectric material before breakdown and t is the thickness of the capacitor.

At low field strengths there exists a limited group of charge carriers due to electronic or ionic imperfections in the capacitor. As the field strength rises, the conductivity of the capacitor increases, promoting more electrons to pass through the capacitor until the breakdown. As the capacitor reaches the breakdown, two phenomena contribute to the dielectric rupture: an electronic breakdown and a thermal breakdown [26].

Electronic breakdown takes place when a localized voltage reaches the maximum value that causes the overall capacitor breakdown. However, thermal breakdown occurs by a localized overheating produced by the electrical field. Higher electrical conductivity due to the higher temperature increases the channels of currents passing through the sample, which produce a local instability and the final capacitor rupture.

2.5.3 Resistivity

Electrical resistivity is the ability of dielectric materials to withstand the flow of electrical current. Thus, dielectric materials with high resistivity hinder the flow of electrical current [26]. This electrical property is the inverse of the conductivity, which takes the electrical

current density into consideration. For dielectric materials, the resistivity is given by equation 9 [26].

$$\rho = \frac{1}{\sigma} \quad (9)$$

σ is the conductivity of the dielectric material. If the electrical current density is defined as the charge transported through the cross sectional area of the capacitor, the electrical conductivity can be expressed by equation 10 [26].

$$\sigma = \frac{j}{E} \quad (10)$$

E is the electric field strength and j is the current density. Both electrical properties are given by equation 11 and 12, respectively [26].

$$E = \frac{V}{t} \quad (11)$$

$$j = \frac{i}{A} \quad (12)$$

V is the voltage through the capacitor, t is the thickness of the dielectric material, i is the current through the plates and A is the cross sectional area of the capacitor.

2.6 Thermomechanical Analysis

2.6.1 Glass Transition Temperature (T_g)

Polymer crystallinity is an important property for all polymers. There are three different types of polymer rearrangement such as crystalline, semi-crystalline and amorphous. For crystalline polymers, the molecules are orderly rearranged, which made the polymer more rigid. When polymers have both amorphous and crystalline regions, it is known as semi-crystalline polymer. In an amorphous polymer, the molecules are oriented randomly and are intertwined. Figure 6 shows the schematic of crystalline and amorphous phases in a semi-crystalline polymer.

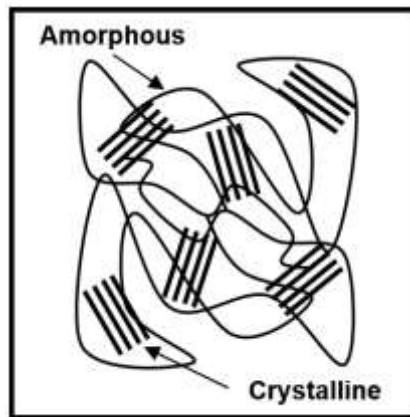


Figure 6. Crystalline and amorphous phases in a semi-crystalline polymer.

Polymer crystallinity affects the glass transition temperature (T_g), which relates with the thermal energy required to change the molecular conformation of the polymer structure. Below the T_g , the molecular conformation remains in the glassy state where the polymer is hard and brittle. When the temperature rises above the T_g , the polymer is in the rubbery state where it becomes soft and flexible.

In order to determine the T_g from a strain vs. temperature curve (obtained via thermomechanometry) tangent lines are drawn to both the glassy and rubbery parts of the curve (Figure 7). The intersection between both tangents is known as the glass transition temperature. This glass transition is exhibited for the amorphous portion of a semi-crystalline polymer since the crystalline portion remains crystalline during the glass transition.

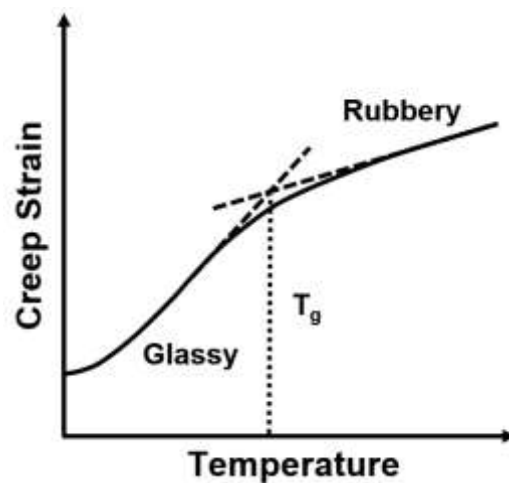


Figure 7. Strain of a polymer as a function of the temperature.

2.6.2 Creep Analysis

In the study of reinforced polymers a relevant mechanical behavior is creep, which is understood as the deformation of the polymer at a constant load at a given temperature. To study creep behavior at constant load and temperature, the material strain is measured as a function of time. A typical creep strain curve consists of three stages. Before the primary stage, an instantaneous deformation occurs at constant load as a function of the elastic modulus of the material at the experiment temperature. Subsequently, the deformation of the polymer increases upon the primary stage. In the

secondary creep stage, a steady state linear deformation is observed, which is followed by an accelerated deformation (tertiary stage) until the fracture occurs.

For instance, the creep deformation depends of the load and the temperature applied to the polymer, the time of deformation, and the structure and morphology of the polymer. Additionally, the creep deformation can be affected by the addition of particles, interphase between the particles and the polymeric matrix, and the dispersion of the particles. Researchers normally model the creep deformation of these viscoelastic materials using a series of linear springs and linear dashpots. The spring element exhibits the elasticity and recovery of the material (equation 13), while the dashpot represents the viscous behavior of the material (equation 14).

Figure 8 shows the spring and dashpot elements utilized to model the creep deformation of the materials.

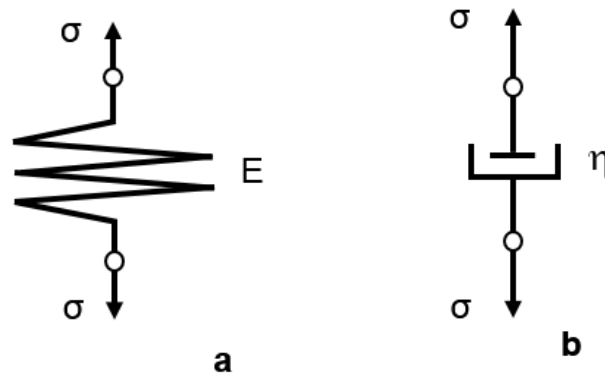


Figure 8. (a) Spring element and (b) dashpot element.

$$\sigma = E \cdot \epsilon \quad (13)$$

$$\sigma = \eta \frac{d\epsilon}{dt} = \eta \dot{\epsilon} \quad (14)$$

E is the Young's modulus, ε is called as the creep strain, η is known as the coefficient viscosity and $\dot{\varepsilon}$ is the creep strain rate.

The linear springs and linear dashpots can be arranged in series or parallel to formulate different models. In particular, the Maxwell model consists of springs and dashpots connected in series while the Kelvin model a parallel arrangement of spring and dashpots, as shown in Figure 9. As consequence, the overall strain for elements connected in series is given by equation (15).

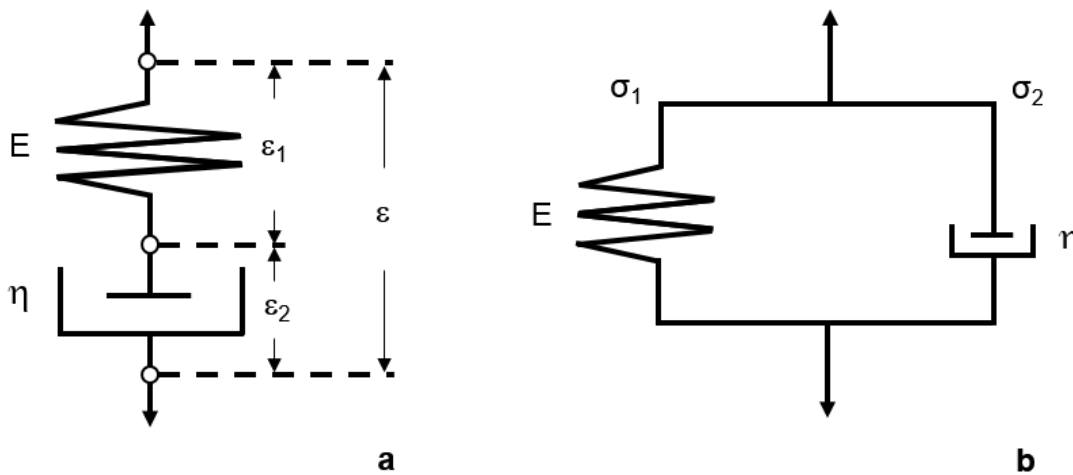


Figure 9. (a) Maxwell model and (b) Kelvin model.

$$\varepsilon = \varepsilon_s + \varepsilon_d \quad (15)$$

ε_s and ε_d are the strain of the spring and dashpot, respectively. These variables are expressed in terms of stress. As a result, the strain response is given by equation 16.

$$\varepsilon(t) = \frac{\sigma}{E} + \frac{\sigma}{\eta} t \quad (16)$$

σ is the applied stress, η is the coefficient of viscosity, E is the Young's modulus and t is the time under the applied load.

In the Kelvin model, the springs and dashpots are connected in parallel. Since both elements are arranged in parallel, the cumulative stress is given by equation 17.

$$\sigma = \sigma_s + \sigma_d \quad (17)$$

σ_s and σ_d are the stress of the spring and dashpot, respectively. The creep strain response under a constant stress is given by equation 18.

$$\varepsilon = \frac{\sigma}{E} [1 - \exp(-E \cdot t / \eta)] \quad (18)$$

Based on the discussion of the Maxwell and Kelvin models, we are able to express the Burger's model in equation 19.

$$\varepsilon = \frac{\sigma}{E_1} + \frac{\sigma}{E_2} [1 - \exp(-E_2 \cdot t / \eta_2)] + \frac{\sigma}{\eta_1} t \quad (19)$$

Moreover, the shear creep compliance $J(t)$ is an important characteristics for polymers. This compliance is defined as the change in strain as a function of time under a constant stress, equation (20) [28].

$$J(t) = \frac{\varepsilon_2(t) - \varepsilon_1(t)}{\sigma_0} \quad (20)$$

ϵ is the strain as a function of time and σ_0 is the constant stress applied. By writing equation 19 in terms of shear creep compliance, equation 21 is obtained.

$$J = \frac{1}{E_1} + \frac{1}{E_2} [1 - \exp(-E_2 t / \eta_2)] + \frac{t}{\eta_1} \quad (21)$$

Equation 21 states the response of the polymer under a constant stress and temperature. The study of the thermomechanical properties of the bio-composites is necessary. These bio-composites are placed inside or between metallic plates, which then are placed in an electrical circuit. All these factors produce tension or compression effects in the bio-composites. Additionally, the applied electric field produces temperature changes in the capacitors. Thus, we decided to study the mechanical properties of the bio-capacitors under tension and at two different temperatures.

3 EXPERIMENTAL PROCEDURE

The experimental procedure is divided in two parts. The first part consists of the fabrication of chitosan-cellulose polymeric films while the fabrication of bio-ferroelectric composites is presented in the second part. The composites then underwent a series of structural, mechanical and thermal analysis. Furthermore, dielectric properties have been measured.

3.1 Materials Selection

To fabricate the polymer films we used poly (D-glucosamine) deacetylated chitosan, i.e. $(C_6H_{11}O_4N)_n$ (with 75% deacetylation provided by Sigma Aldrich), cellulose powder (cotton linsens also provided by Sigma Aldrich), strontium titanium oxide, i.e. $SrTiO_3$ (99+%, provided by Fisher Scientific). The chitosan solution was prepared using acetic acid glacial CH_3CO_2H (99.7+%, obtained from Alfa Aesar). Moreover, 4-methylmorpholine N-oxide solvent $C_5H_{11}NO_2$, (50wt% in water, provided by Sigma Aldrich) was required to complete the cellulose solution. In the next section, the fabrication of the nanocomposites is presented.

3.2 Fabrication of Chitosan-Cellulose Polymeric Films

The polymeric films consisted of a mixture of two biopolymers: chitosan and cellulose, obtained by a solution casting method in which the solution was placed onto petri dishes and dried. For the chitosan solution, the polymer was dissolved into an acetic acid aqueous solution and mechanically stirred. We decided to limit the concentration of chitosan to 1.5 v% because in preliminary experimentations higher concentrations were

found to increase the viscosity of the solution to unmanageable conditions. Additionally, different percentages of acetic acid concentration were used in order to determine if the mechanical properties of the films were affected, particularly when using 1.25 v% and 2.50 v% acetic acid.

The cellulose solution was prepared by the addition of the polymer into 4-methylmorpholine N-oxide (NMMO) solvent and mechanically stirred at 65°C to favor more solubility of the polymer. As previously stated, a solvent is required to dissolve cellulose because its structure consists of three hydroxyl groups, which make a complex pattern of hydrogen bonds [29]. In our study two cellulose concentrations were analyzed, 0.5 v% and 1.0 v%, in order to evaluate the effects of different concentration of cellulose in the composite.

After the stock solutions of chitosan and cellulose were prepared, two batches of films were produced. In the first batch, the concentration of cellulose was set to 0.5 v% while 1.0 v% was adjusted for the second batch. Each batch consisted of three small solutions containing, 5 v%, 15 v% and 25 v% of cellulose.

The smallest solutions were mechanically stirred and poured into petri dishes, and dried in an oven at 40°C. Afterward, the films were removed from the petri dishes using a basic solution. Since upon the films removal, they absorbed a great amount of water, a second dry process was necessary. Figure 10 shows the experimental procedure for the fabrication of chitosan-cellulose films.

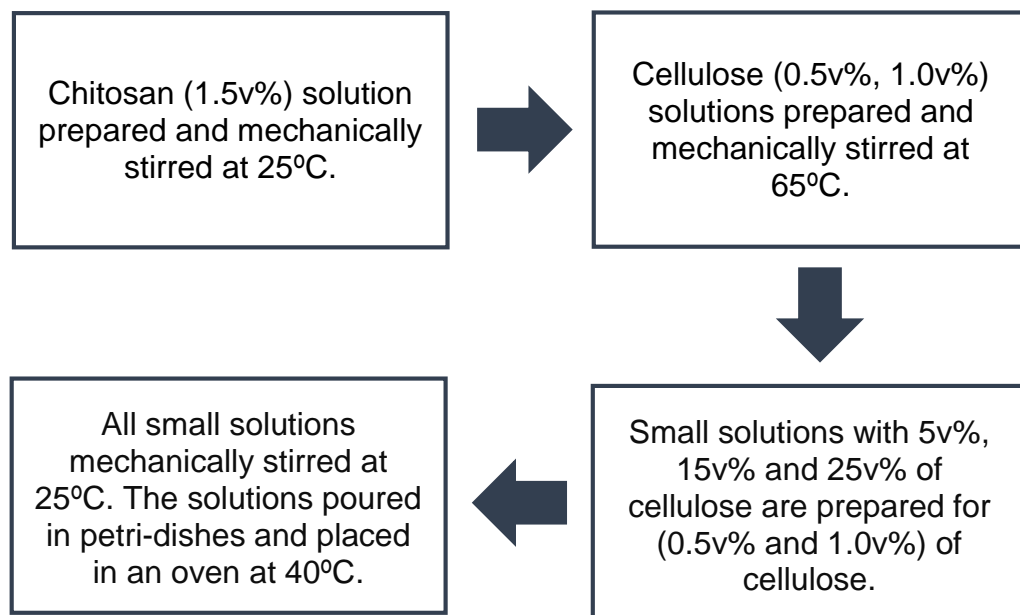


Figure 10. Sequence of the fabrication of chitosan-cellulose films.

3.3 Fabrication of Bio-Ferroelectric Composites

Bio-ferroelectric nanocomposites were developed layer by layer via the solution casting method. Initially, they had been prepared by adding the nanoparticles into each smaller chitosan-cellulose solution presented in the previously section. However, the nanoparticles bearing a density of 5.118 g/cm^3 , i.e. three times the density of the polymer, settled at the bottom of the solution, which affected the dispersion of the particles. Therefore, to improve the dispersion of the nanoparticles, we deemed necessary to fabricate a composite with a chitosan-cellulose layer followed with a polymer-nanoparticles layer.

The first layer of the nanocomposite was prepared from a chitosan-cellulose solution, where the polymer was dissolved in an aqueous solution with acetic acid and mechanically stirred at room temperature. The cellulose was dissolved in a 4-

methylmorpholine N-oxide solvent under vigorous stirring at 65°C. After the stock solutions were completed, two small solutions with different volume percentages (15 v% and 25 v%) of cellulose were produced, poured into petri dishes and placed in an oven at 40°C. In the fabrication of the bio-ferroelectric composites, 5 v% solution was not used since the composites underwent crazing when the films were removed using a basic solution.

For the second layer, other stock solutions of chitosan and cellulose were prepared. Cellulose and strontium titanate nanoparticles were added into that chitosan solution to formulate the smallest solutions, which were sonicated and mechanically stirred to disperse the nanoparticles that otherwise would have agglomerated in the solution. Such agglomeration is caused by strong van der Waals forces between the nanoparticles [30]. The amounts of the nanoparticles selected to analyze their effects in the mechanical and electrical properties were 10 wt% and 20 wt%. The solutions were poured onto the first layer of chitosan-cellulose and placed in an oven at 40°C. Finally, the films were removed from the petri dishes with a basic solution and let dry to remove the excess of water present in the composite. Figure 11 shows the experimental procedure for the fabrication of the bio-ferroelectric nanocomposites.

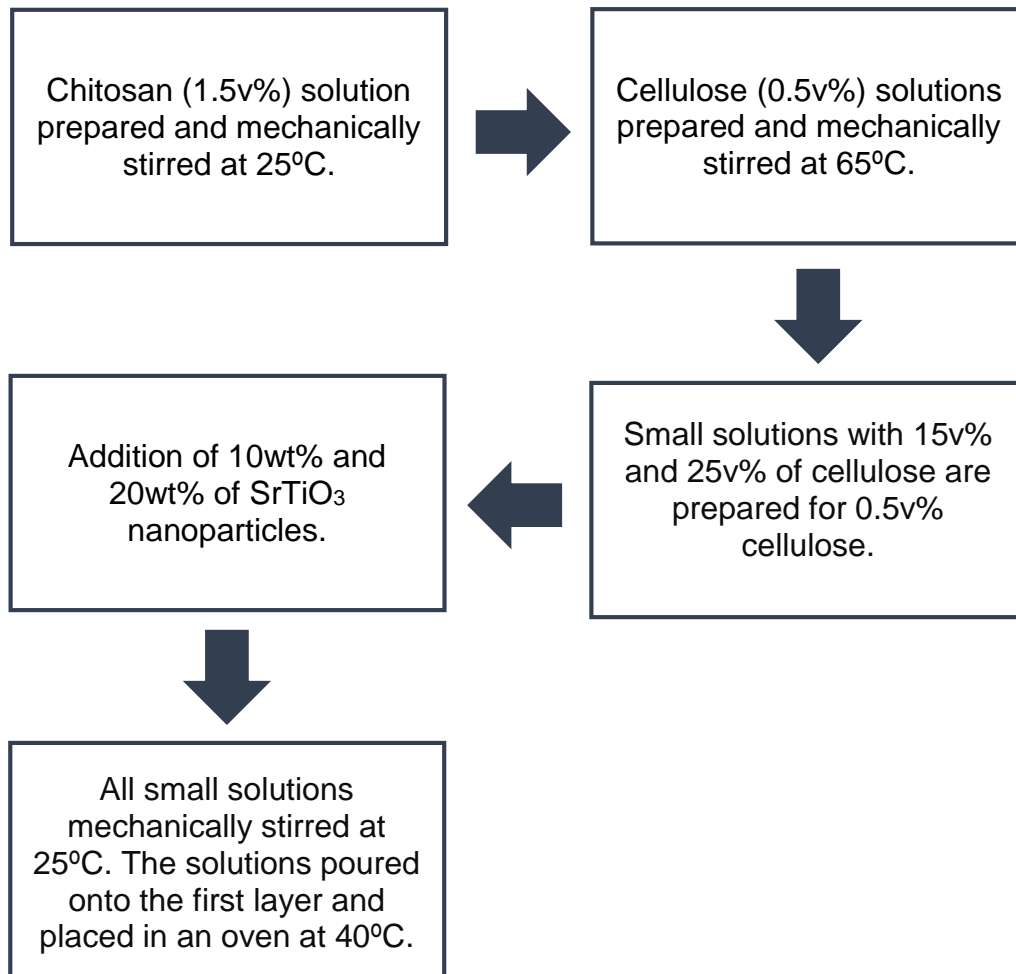


Figure 11. Experimental procedure of the fabrication of chitosan-cellulose films with ferroelectric nanoparticles.

As presented, these bio-ferroelectric nanocomposites consisted of 0.5 v% of cellulose. Composites with 1.0v% of cellulose were not considered due to the negative effect in the mechanical and thermal properties obtained for the chitosan-cellulose films.

3.4 Materials Characterization

3.4.1 Structure Analysis

- The samples structures were characterized via x-ray diffraction, which provides crystalline structural information such as the average size of the nanoparticles and the crystalline phases present in the composites. The average size of the nanoparticles was obtained through the Scherrer's equation [31]. All samples were characterized with a Rigaku ULTIMA III diffractometer operated at 40 kV and 44 mA. The diffraction patterns were collected at 25°C with a 2θ step of 0.02° and a dwell time of 1 second. The target used was copper with a $K\alpha$ wavelength of 0.154178 nm.
- Additionally, Fourier transform infrared spectroscopy (FTIR) was used to analyze the structure of the samples. The FTIR unit emits light in the infrared region in order to study the vibrations and rotations of the bonds present in the sample. The energy provided by the FTIR is absorbed at the frequency of the bonds between the atoms, allowing its identification. All samples were analyzed with a Shimadzu IRAffinity-1 at a range of 4000 cm^{-1} to 600 cm^{-1} . For each run, the accumulation of scans was 200 at a resolution of 4 cm^{-1} .

3.4.2 Mechanical Analysis

- A thermomechanical analyzer (TMA) allowed studying the deformation of the composite materials as a function of time, as well as their glass transition temperatures (T_g). In addition, this TMA allowed evaluating the elastic behavior of the bio-composite, including the shear creep compliance. To determine these

properties, 10 mm long by 5 mm wide samples underwent a temperature ramp of 5°C/min from 25°C to 300°C in an air atmosphere. The applied force was 1.0 N, which was kept constant during each run. In this case, the composite underwent a 1.0 N load at two temperatures, 25°C and 100°C, for 3 hours. All these properties were measured using a TMA/SDTA84e from Mettler Toledo thermomechanical analyzer.

- All samples were characterized in a low force universal testing machine Instron® model 5944 to determine their ultimate tensile strength. The deformation velocity was set to 1mm/min at room temperature (25°C). For the dimensions of the samples, the ASTM D-1708 standard was used: 22mm gauge length, 5mm wide and 5mm radius fillet.

3.4.3 Thermal Analysis

- A TGA/SDTA from Mettler Toledo thermogravimetric analyzer (operated at a temperature ramp of 5°C per minute from 25°C to 500°C) helped to determine properties such as degradation temperature (T_{deg}). The samples were placed on a balance that records the mass loss of the samples as a function of temperature. To determine the degradation temperature, the first derivate of the mass loss vs temperature was obtaining from the TGA/SDTA analyzer; the degradation temperature was the minimum value of the first derivate.

3.4.4 Electrical Analysis

- The electrical properties measured included capacitance and the current passing through the dielectric material. The capacitance was measured using a QuadTech 2200 automatic transformer test system (with an AC supply) as a function of the frequency, set from 1 kHz to 10 kHz. Subsequently, the dielectric constant as a function of the frequency was determined from the capacitance.
- A GW INSTEK GPS-3303 DC power supply permitted to assess the current passing through the dielectric material when the applied voltage changed between 5V and 60V and a GW-INSTEK GDM-8246 power meter connected in series was used to collect the electrical current values. A step-by-step method was implemented, i.e. the applied voltage was raised at equal increments for a specific time. Increments of 5V were applied to the capacitor and then, after 10 seconds, the current flow was recorded at each one of the 5V increments.
- In order to develop a capacitor, an XLX sputter unit applied a titanium coating on both nanocomposite sides for 20 minutes at 200 watts. All these capacitors were characterized using a Calframo™ stirrer clamp made of cast zinc-aluminum alloy coated with epoxy, as shown in Figure 12. This clamp included a hold chuck key in which a copper electrode was placed. In addition, another copper electrode was placed at the base of the Calframo™ stirrer clamp. Then the electrical properties were measured by placing the capacitor between the two copper electrodes as a 1.27 N load was applied on the capacitors to ensure proper contact. For the dimensions of the samples, we used the ASTM D-150 standard, which requires a 10 mm length and 10 mm wide specimen [32].



Figure 12. Calframo™ stirrer clamp utilized in the measurement of the dielectric properties.

4 CHARACTERIZATION OF CHITOSAN-CELLULOSE BIO-COMPOSITES

In this chapter, we focused on the study of thermal and mechanical properties of the bio-composites. For this study, the variables considered includes: the concentration of cellulose (0.5 v% and 1.0 v%) and the amount of cellulose (5 v%, 15 v% and 25 v%) added into each small solution. Furthermore, the effects of the acetic acid concentration were analyzed, thus, two concentrations were studied, 1.25 v% and 2.50 v%. In addition, to study the effects of the nanoparticles on the electrical properties of the composites, different percentages of strontium titanate nanoparticles were used: 0 wt%, 10 wt% and 20 wt%.

4.1 Thermogravimetric Analysis (TGA)

The degradation temperature (T_{deg}) was determined from the TGA analysis. The results suggest that higher concentrations of cellulose decreased the degradation temperature of the bio-composites made of chitosan and cellulose (Figure 13). For bio-composites made of 0.5 v% of cellulose, higher T_{deg} values were obtained compared to the 1.0 v% one. Furthermore, the T_{deg} lowered as the amount of cellulose increased from 5 v% to 25 v%.

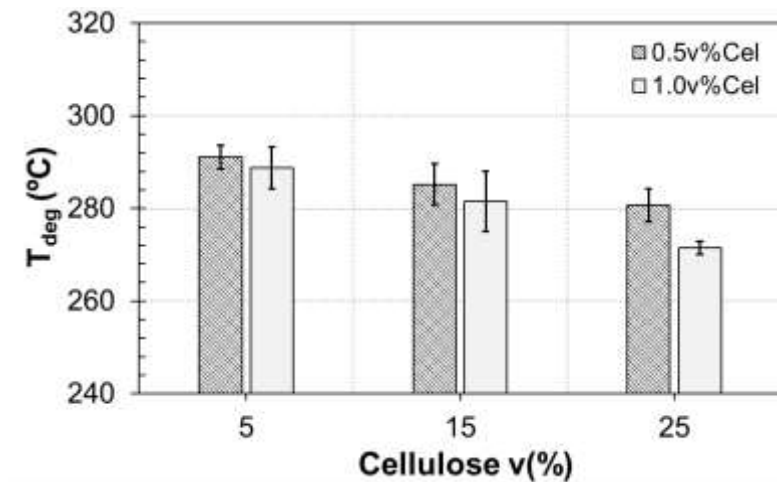


Figure 13. TGA analysis for bio-composites made of 1.5 v% chitosan / (0.5 v% and 1.0 v%) cellulose and 1.25 v% of acetic acid.

As aforementioned, in the fabrication of the bio-composites, cellulose adversely affects the degradation temperature due to the water content in the composites, which depends of the chitosan dissolution in a water/acetic acid medium and the cellulose addition. The interaction between the cellulose hydroxyl groups with the water molecules contributes to the larger presence of water molecules in the polymeric matrix: a) directly linked to the (–OH) groups or b) confined between the polymer chains due to the hydrogen bonds formed by the OH groups and the water molecules [33], [34]. To remove the water content in the polymer, higher temperatures are required in the drying process but those can affect the chemical structure of the polymer.

In addition, the effects of the acetic acid concentration on the degradation temperature were also studied. For bio-composites made of 1.25 v% and 2.50 v% of acetic acid, the addition of cellulose lowered the T_{deg} of the composites. However, lower values of T_g were obtained for 2.50 v% acetic acid concentration compared than 1.25 v%, as shown in Figure 14.

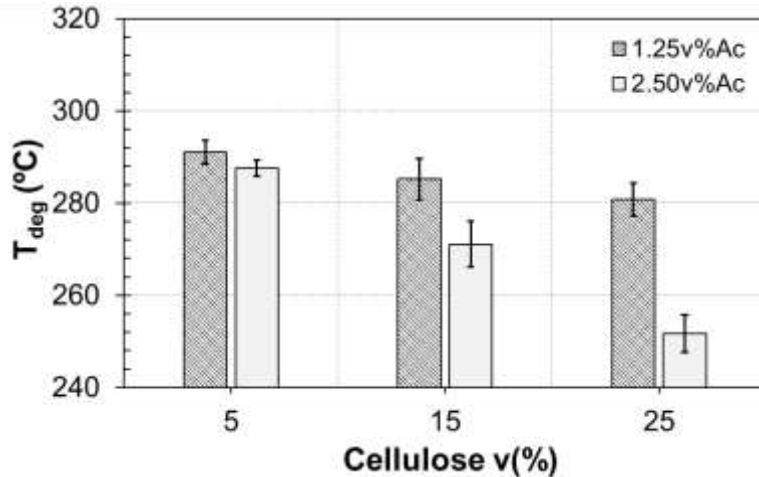


Figure 14. TGA analysis for bio-composites made of 1.5v% chitosan / 0.5v% cellulose considering 1.25v% and 2.50v% of acetic acid.

Higher concentrations of acetic acid lowered the T_{deg} due to the swelling degree of the composites. Hosokawa et al. stated that the swelling degree depends of the crosslinking between chitosan and cellulose, which can originate from the Schiff base reaction. In the Schiff base reaction, the hydrogen ions of the primary amino groups of chitosan ($-NH_2$) interacts with the aldehyde groups ($-COH$) in the cellulose leading the formation of ($-CH=N-$) groups at pH 6.0 [7], [35], [36]. In other words, at pH 6.0, the amine groups are partially deprotonated. When the pH is below than 6.0, the amine groups ($-NH_2$) are fully protonated in the form of (NH_3^+); increasing the electrostatic repulsion between the polymer chains. Higher electrostatic repulsions allow more water molecules between the polymer chains. Thus, the swelling degree increases, resulting in a lower cross-linking degree of the polymer chains.

4.2 Tensile Analysis

One of the mechanical properties analyzed was the ultimate tensile strength (UTS), which i.e. the maximum stress that the bio-composites can withstand before the rupture. Figure

15 suggests that higher concentrations of cellulose diminished the ultimate tensile strength. For 0.5 v% and 1.0 v% of cellulose, the UTS lowered 3.5 MPa, as the amount of cellulose increased from 5 v% to 25 v%. In addition, the effects of the acetic acid concentration were also analyzed. For bio-composites made of 1.25 v% and 2.50 v% of acetic acid, the UTS diminished as the amount of cellulose increased from 5 v% to 25 v%, as shown in Figure 16. When the acetic acid concentrations were compared, a reduction of 7 MPa was observed for 5v%, 15v% and 25v% of cellulose, as evidenced in Figure 16.

As stated in the previous section, higher amounts of cellulose and acetic acid increase the water content in the polymer films. Cellulose possesses three hydroxyl groups, which interact with the water molecules while the acetic acid increases the electrostatic repulsions between the polymer chains at pH values below 6.0. As a result, there is an increase of the water content between the polymer chains.

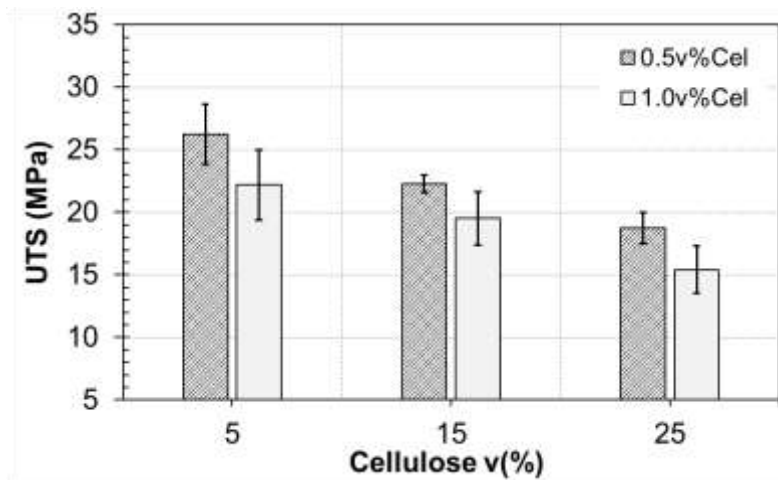


Figure 15. Tensile analysis for bio-composites made of 1.5 v% chitosan / (0.5 v% and 1.0 v%) cellulose and 1.25 v% of acetic acid.

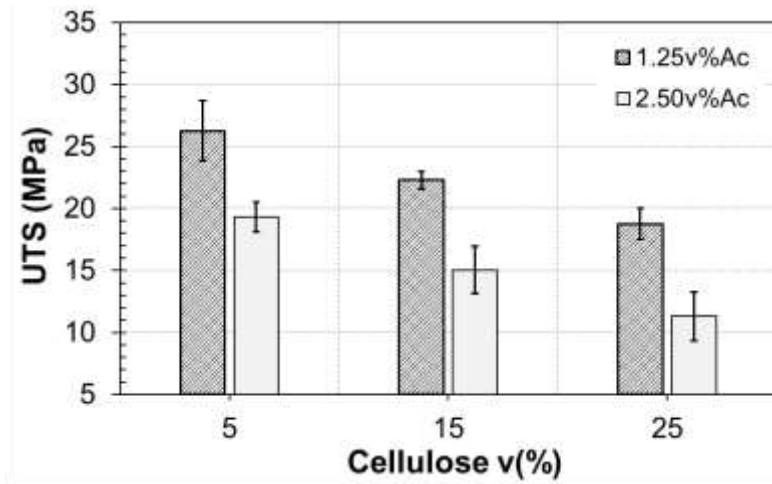


Figure 16. Tensile analysis for bio-composites made of 1.5 v% chitosan / 0.5 v% cellulose considering 1.25 v% and 2.50 v% of acetic acid.

5 CHARACTERIZATION OF BIO-FERROELECTRIC NANOCOMPOSITES

In order to perform a more exhaustive study of the thermal, mechanical and electrical properties, we evaluated the percentage of cellulose (15 v% and 25 v%) and the amount of particles incorporated into the nanocomposites; i.e. 10 wt% and 20 wt%. Contrary to the variables considered in Chapter 4, 5 v% of cellulose was not considered because the polymeric films started experiencing crazing effect at that level of cellulose. For the acetic acid concentration, it was set to 1.25 v% because higher thermal and mechanical properties were obtained for 1.25 v% than for 2.50 v% of acetic acid.

5.1 SrTiO₃ Nanoparticles

According to the literature, reinforcing particle size affects the mechanical, thermal and electrical properties of similar composites [37]. In our case, to enhance the nanoparticles dispersion in the matrix, their size was reduced using a Vario-Planetary Ball Milling Pulverisette 4 Fritsch™. Since this technique can create impurities, the crystalline structure of the STO powder was analyzed using XRD. The resulting diffractogram, shown in Figure 17, matched with the expected STO pattern without the presence of impurities.

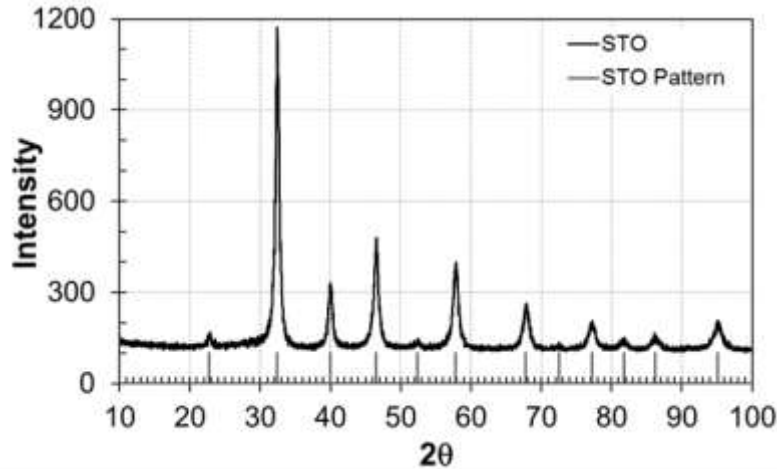


Figure 17. XRD pattern of STO powder after 10 hours of milling.

The particle size of the ball milled STO powder was determined at different milling times using the Scherrer equation, based on the width of the largest XRD peak [31], [38]. Before milling, the particle size ranged between 40 to 50 nm, and decreased to 18 nm after 5 hours of milling (Figure 18); after that time it did not show a significant change. According to previous findings, as the particle size is reduced, the agglomeration of the particles diminishes, improving the mechanical, thermal and electrical properties of the nanocomposites [37], [39]. When the particle size reach the microscale, the particles tend to agglomerate due to the electrostatic forces acting in each particle.

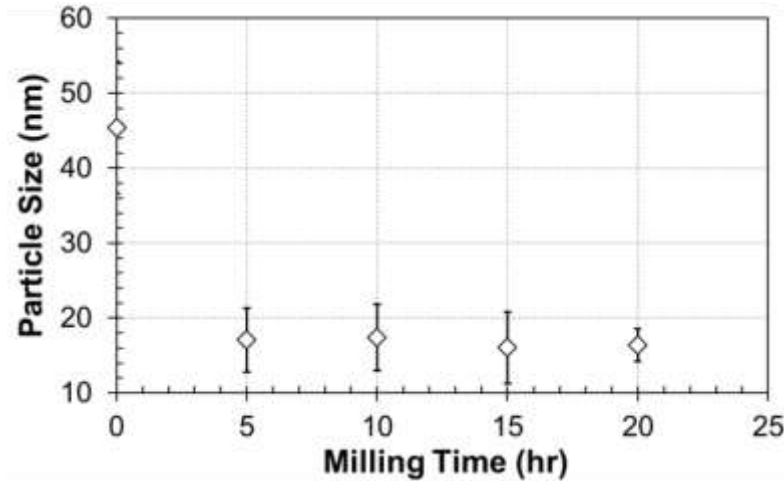
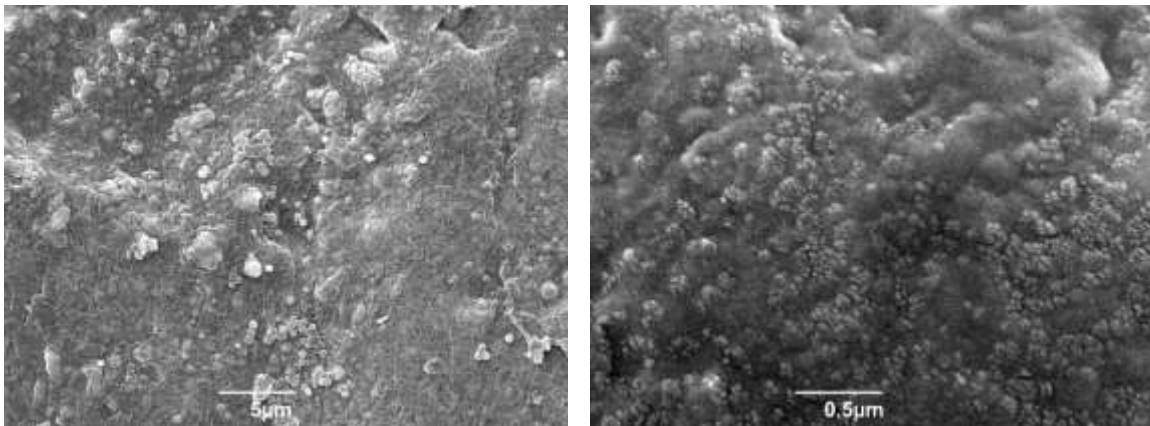


Figure 18. STO particle size as a function of milling time.

After mixing with the polymer, the dispersion of the nanoparticles was observed using a scanning electron microscope (Figure 19). At low magnification, STO agglomerates are observed on the polymer surface. Even though there is STO agglomeration, the dispersion of the nanoparticles was enhanced, as shown in Figure 19b, obtained at higher magnification.



(a)

(b)

Figure 19. Scanning electron microscopy images obtained from a bio-ferroelectric nanocomposite (20 wt% STO): (a) low magnification; (b) high magnification.

5.2 Thermogravimetric Analysis (TGA)

As discussed before, the degradation temperature of the nanocomposites was analyzed via TGA. The results suggest that the degradation temperature raised as the volume percentage of cellulose increased, contrary to the observed behavior for the bio-composites without nanoparticles, as shown in Figure 20. The presented behavior could be due to charge interactions between the STO nanoparticles and the polymeric chains. Furthermore, higher percentages of STO nanoparticles lowered the T_{deg} of the composites.

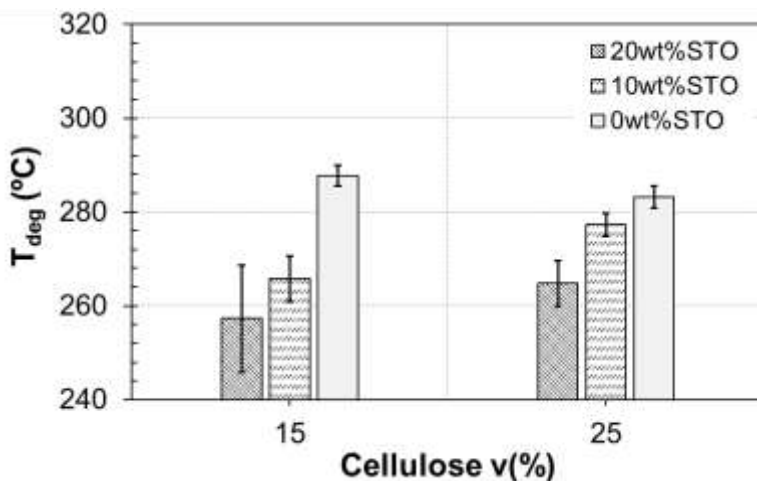


Figure 20. TGA analysis for bio-composites made of 1.5 v% chitosan / 0.5 v% cellulose considering 20 wt%, 10 wt% and 0 wt% of strontium titanate nanoparticles.

Even though the addition of STO nanoparticles slightly increased the T_{deg} of the composites, larger amounts of nanoparticles greatly lowered the T_{deg} , as evidenced by comparing 0 wt% and 20 wt%. At low nanoparticle content, the interfacial adhesion polymer-nanoparticles dominates. To promote thermal stability, it is required to utilize a nanoparticle content above 30 wt% [40]. Additionally, the T_{deg} is affected by the agglomeration of the nanoparticles, which reduces the polymer-nanoparticles interfacial

bonding. Furthermore, in another research, the nanoparticles were found to increase the presence of pores in the polymeric matrix, affecting the interaction between the nanoparticles and the polymer [39].

5.3 Tensile Tests

As shown in Figure 21, the UTS raised as the amount of cellulose increased from 15 v% to 25 v% for the composites containing STO nanoparticles, contrary to the behavior observed for composites without nanoparticles. When the UTS values for the composites are compared, the UTS values increased as the percentages of STO nanoparticles decreased from 20 wt% to 0 wt%.

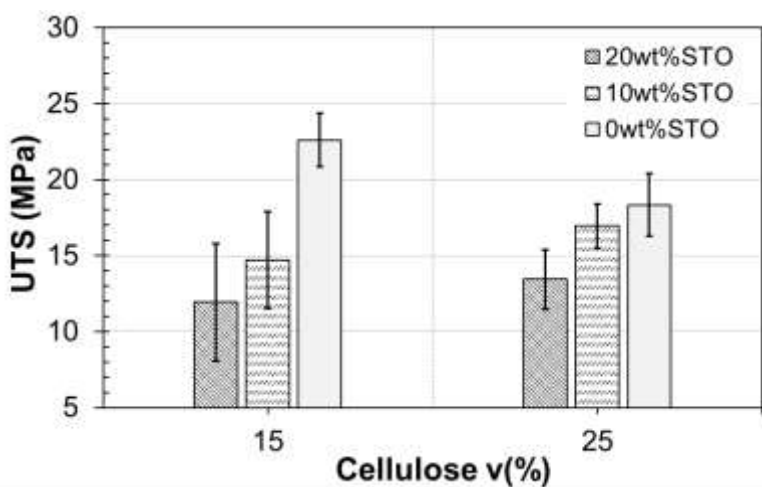


Figure 21. Tensile analysis for bio-composites made of 1.5 v% chitosan / 0.5 v% cellulose considering 20 wt%, 10 wt% and 0 wt% of STO nanoparticles.

As stated in the TGA section, the addition of cellulose and STO nanoparticles slightly increased the pH values of the solutions; improving the interaction between chitosan and cellulose. This interaction reduced the amount of water in the resulting polymeric films.

However, larger amounts of STO nanoparticles decreased the UTS of the composites; even though increased the pH of the solution.

There are a number of factors that could affect the mechanical properties of the composites: particle content, particle size, particle structure and particle dispersion [39]. For instance, higher percentages of nanoparticles increase the polymer-nanoparticles interfacial energy, which causes cracks through the nanoparticles in the polymeric matrix. Additionally, as mentioned in the TGA section, the agglomerates of nanoparticles adversely affected the polymer-nanoparticle interfacial bonding. The agglomerates can increase the presence of pores and nucleate microspaces through the nanoparticles, raising the brittleness of the composites.

5.3.1 Thermomechanical Analysis

5.3.1.1 Glass Transition Temperature

Figure 22 shows that T_g did not appear to significantly change as the volume percentage of cellulose increased from 5 v% to 25 v% when no STO nanoparticles are present. The glass transition temperature of the bio-composites ranged between 210°C to 220°C.

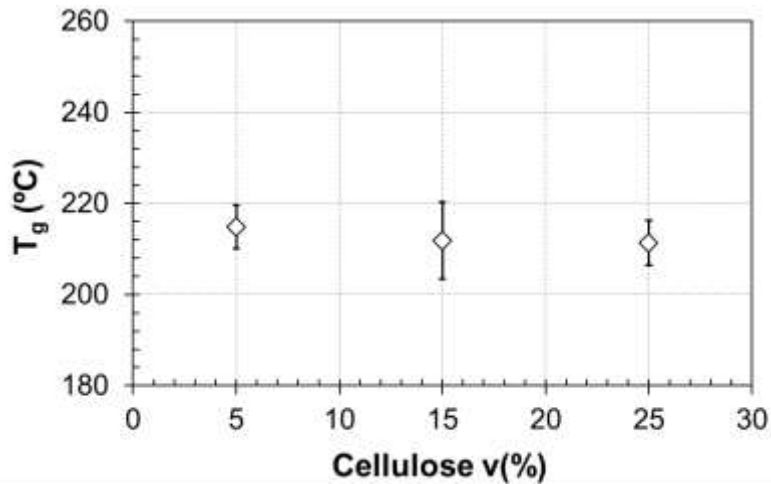


Figure 22. Glass transition temperature (T_g) for biopolymers made of 5 v%, 15 v% and 25 v% of cellulose.

When the STO nanoparticles were added to the bio-composites, the T_g remains unchanged at high percentage of STO nanoparticles, according to Figure 23 and 24. Again, our results suggest that the cellulose and STO nanoparticles did not affect the glass transition temperature of the composites. In our case, the results approximate the T_g values reported in the literature [41]–[43]. In the literature, the reported chitosan and cellulose T_g varies very much, e.g. from 150°C to 203°C and 180°C to 250°C, respectively [42]. This T_g variation can be due to the polymer source, polymer fabrication, hydrophilic characteristics and even the techniques utilized to measure the T_g [41].

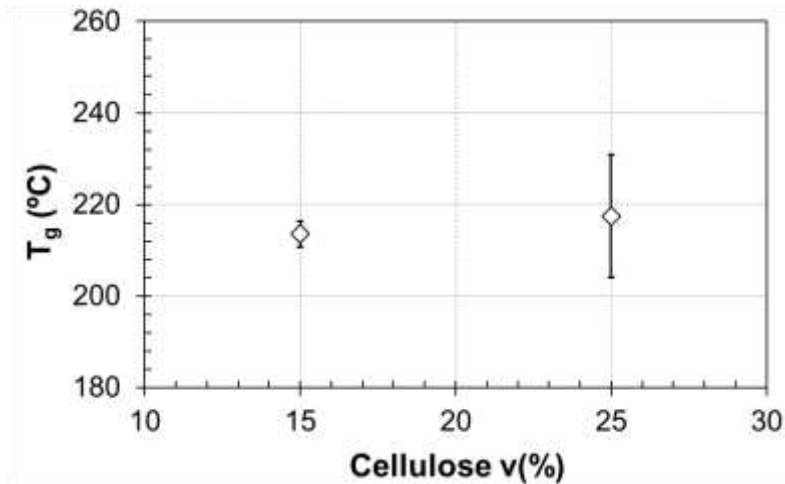


Figure 23. Glass transition temperature (T_g) for bio-composites made of 15 v% and 25 v% of cellulose and 10 wt% STO nanoparticles.

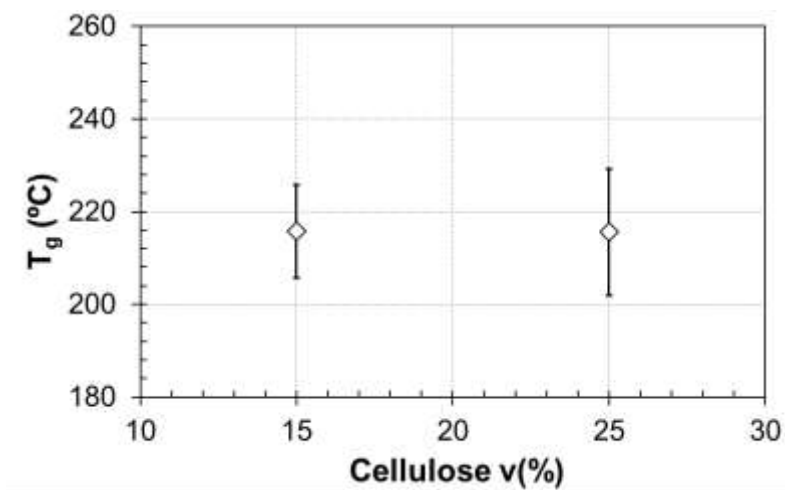


Figure 24. Glass transition temperature (T_g) for bio-composites made of 15 v% and 25 v% of cellulose and 20 wt% STO nanoparticles.

The fact that STO nanoparticles did not appear to change the nanocomposites T_g requires further explanation. When the particles are incorporated into the polymeric matrix, there are some essential elements that could affect the composites T_g , including the extension of the amorphous regions, the extent of the crystallized chains and the interface between nanoparticles and polymeric matrix [44]. In our case, the nanoparticles did not affect the crystallinity of the polymers because the T_g did not change for the chitosan-cellulose

composites and the polymer-STO nanoparticles composites; the T_g values ranged between 210°C and 220°C for all composites. Additionally, the polymer-nanoparticles interfacial energy bonding is not enough to raise the T_g of the composites.

5.3.1.2 Creep Analysis

The creep analysis was performed at two different temperatures and at 1.0 N constant load. In order to observe the effects of the temperature, only 25°C and 100°C were considered since higher deformation occurs around the glass transition temperature of the polymer [28]. In our case, the highest deformation was not observed since the glass transition temperature of the nanocomposites ranged between 210° to 220°C. Thus, our creep analysis took place at a maximum temperature of 100°C, i.e. well below to the glass transition temperature of the polymers.

Creep strain curves as a function of time at 25°C and 100°C are presented in Figure 25 and 26. Two creep stages are apparent in the figures along with the corresponding instantaneous deformations: the primary stage and the unfinished secondary stage. The tertiary stage was not observed, as the time to failure was deemed excessive for the scope of this thesis. Surprisingly though, the overall deformation of the polymer-STO nanoparticles composites was higher than the chitosan-cellulose composites. When no nanoparticles are added, the maximum creep strain for 100°C was 1.8% and 0.6% for 25°C. On the other hand, the creep strain approximates to 2.4% at 100°C and 1.6% at 25°C for composites bearing 20wt% of nanoparticles, respectively. Naturally, the creep strain rose as the temperature increased.

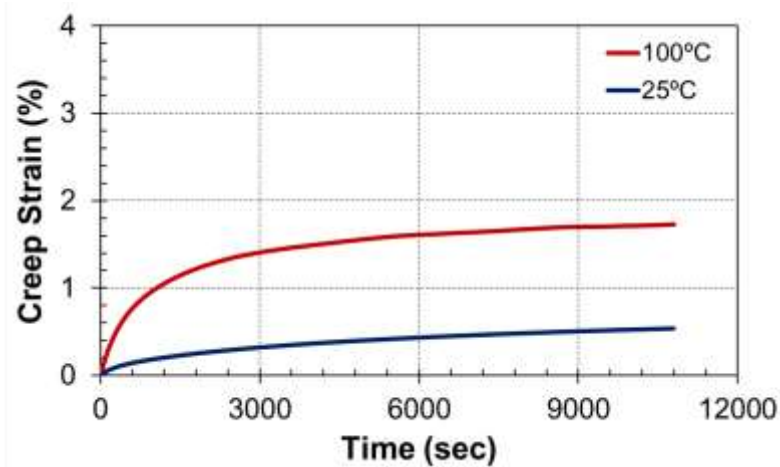


Figure 25. Creep strain as a function of time for a nanocomposite made of 15 v% of cellulose and 0 wt% STO nanoparticles.

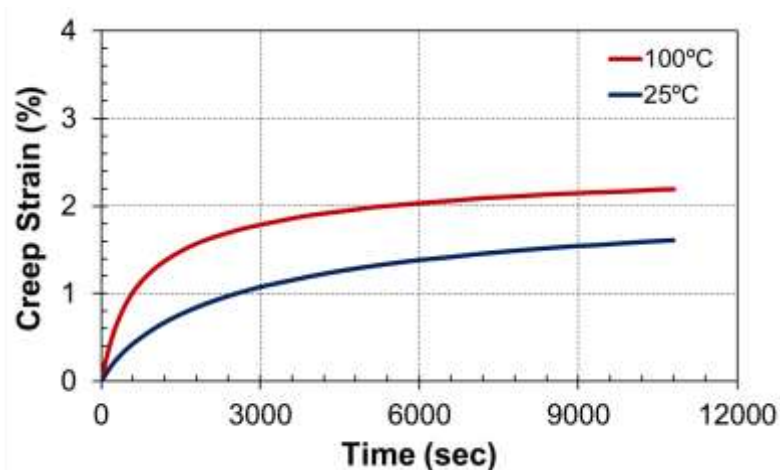


Figure 26. Creep strain as a function of time for a nanocomposite made of 15 v% of cellulose and 20 wt% STO nanoparticles.

Chitosan (present in larger amounts than cellulose in the matrix) possesses high stiffness and resistance to deformation, which was observed upon the tensile analysis. In the presence of nanoparticles in the polymeric matrix, there are essential elements that could affect the creep deformation of the composites: amorphous regions, crystallized chains, interface between nanoparticles and polymeric matrix, polymer-nanoparticles junction,

bridging segments between nanoparticles and dangling polymeric ends, as shown in Figure 27 [44].

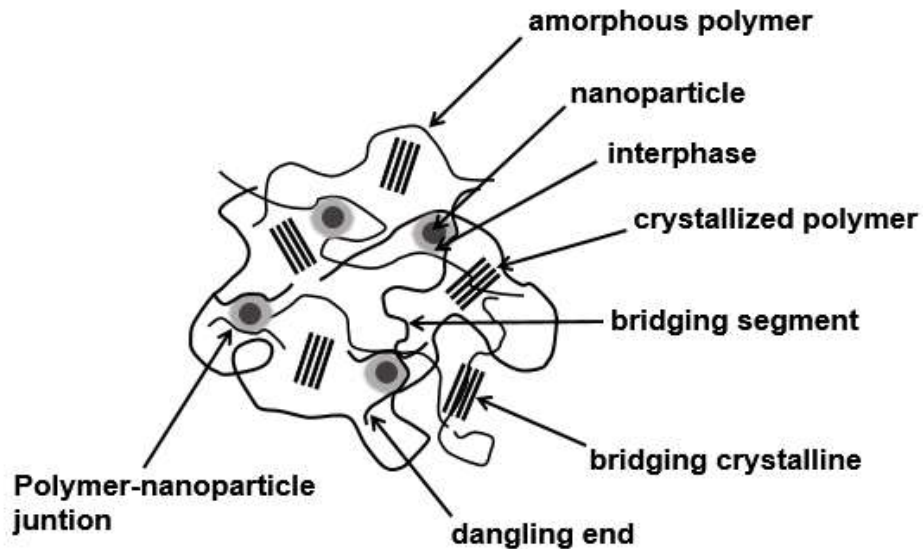


Figure 27. Schematic structure of nanoparticles-semicrystalline polymer composites.

As mentioned, the amorphous and crystalline regions could affect the creep deformation of the composites [44]. Our composites are made of semicrystalline polymers, i.e. with crystalline and amorphous regions. When a load is applied to the crystalline chains, they react rapidly to the mechanical stress and undertake the applied load. However, the amorphous regions take more time to withstand the load. If the polymer has high crystalline regions, the creep deformation is therefore retarded.

The particles presence in the polymeric matrix could have affected the crystallinity of the material; this potential effect was evaluated by comparing the T_g of the polymer and composite. This comparison was presented in the previous section where it was demonstrated the T_g was not significantly altered with the addition of the nanoparticles. Thus, the crystallinity of the chitosan-cellulose and polymer-STO nanoparticles composites remained unchanged.

In our case, the strontium titanate nanoparticles tended to agglomerate due to the electrostatic forces between particles. The polymer-STO nanoparticles interface plays an important role on the creep deformation. The nanoparticles agglomerates could slip at higher shear stresses, resulting in the formation of new cracks around the agglomerates. Under the applied load, the crack propagation likely continued through the polymeric matrix at a slow velocity deformation.

After discussing possible reasons of such anomalous creep behavior, we deemed important to study the viscosity of the solution. We believed that the viscosity of the solution is related to the creep deformation of the composites. Therefore, after determining the Burger coefficients, we analyzed the viscosity effects of the composites. Moreover, the dimensional stability of the nanocomposites was determined by the creep rate, i.e. the velocity of creep deformation (Figure 28 and 29). In the curves obtained, the creep rate, which started at a high value, decreased rapidly with time upon primary creep stage. This reduction of the creep rate could be due to the orientation hardening of the polymer with instantaneous deformation under stress [44]. This was followed by a constant creep rate after 1.5 hours during the secondary creep stage. In this stage, the polymer chains reached a dynamic equilibrium. Naturally, this creep rate is sensitive to temperature; higher temperatures caused higher creep rates. For our composites, the creep rate followed that trend (Figure 28 and 29).

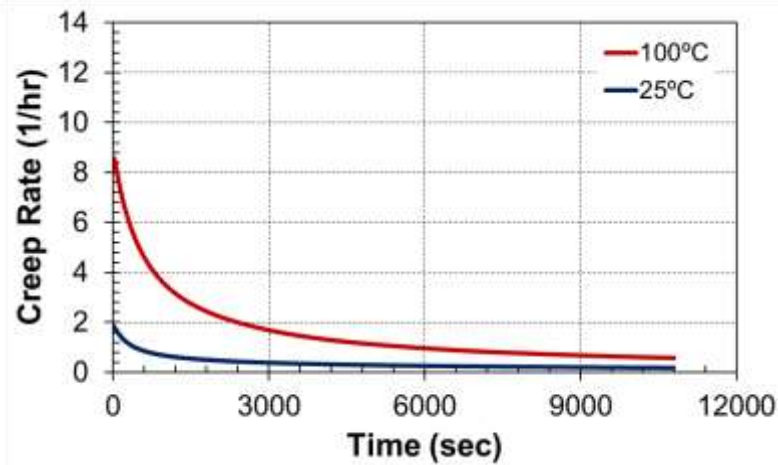


Figure 28. Creep rate as a function of time for a nanocomposite made of 15 v% of cellulose and 0 wt% STO nanoparticles.

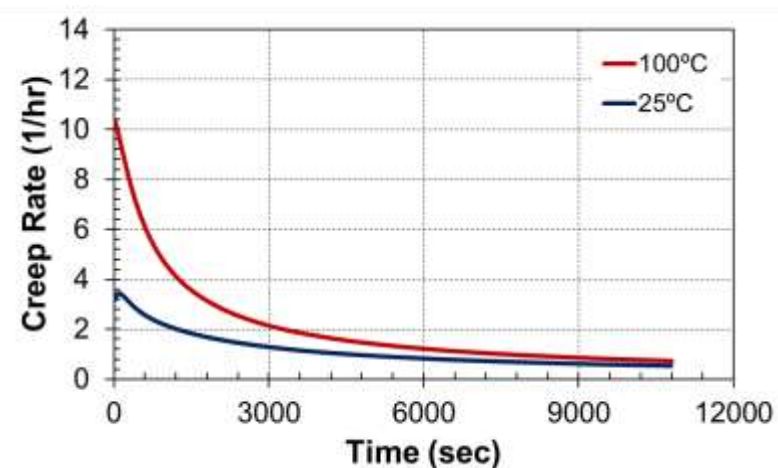


Figure 29. Creep rate as a function of time for a nanocomposite made of 15 v% of cellulose and 20 wt% STO nanoparticles.

The curves of creep compliance as a function of time were obtained under different temperatures and at a constant load of 1.0N (Figure 30 and 31). The creep compliance was studied at 25°C and 100°C; i.e. temperatures below the glass transition temperature of the chitosan and cellulose. Evidently at 100°C, the creep compliance of each composite was greater than at 25°C. Higher temperatures increase the mobility of the polymer chains; increasing the creep deformation of the material.

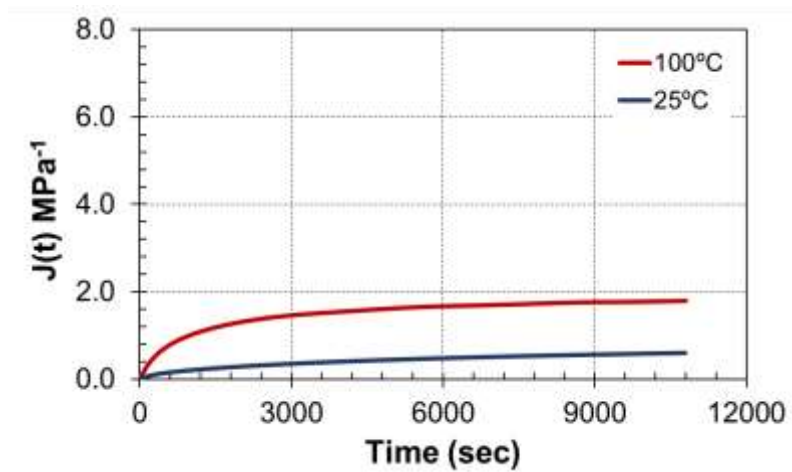


Figure 30. Creep compliance as a function of time for a nanocomposite made of 15 v% of cellulose and 0 wt% STO nanoparticles.

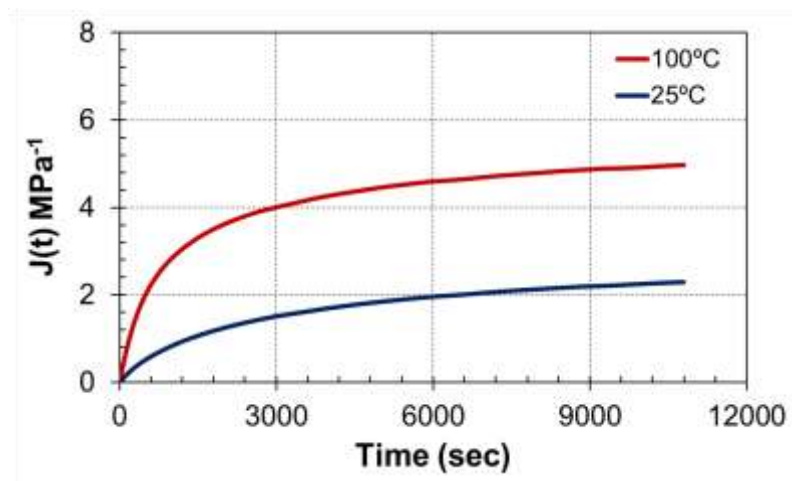


Figure 31. Creep compliance as a function of time for a nanocomposite made of 15 v% of cellulose and 20 wt% STO nanoparticles.

After analyzing the creep compliance at 25°C and 100°C, we computed the Burger coefficients E_1 , E_2 , η_1 and η_2 to finally obtain the creep compliance equation for each condition (Table 6 and 7). The Box-Lucas regression model is given by $y = a(1 - \exp^{-bx})$ while $y = mx + b$ represents the linear regression model. The Burger coefficients, E_1

represent the elastic recovery since E_2 represent the rubbery elasticity of the bio-composites. The η represent the viscosity coefficient of the bio-composites.

At 100°C, the E_1 values for 0 wt% STO nanoparticles were higher than for 20 wt% STO nanoparticles, which means that the instantaneous deformation was lower for the bio-composites without nanoparticles. In other words, the polymer-STO nanoparticles composites suffered more deformation under an applied load and temperature. Similarly, the E_2 values for 0 wt% STO nanoparticles were higher than for the bio-composites containing the strontium titanate nanoparticles resulting in high permanent deformation. Conversely, the coefficients of viscosity (η_1 and η_2) lowered for the composites made of STO nanoparticles, and thus, the permanent creep strain increased. When η_1 and η_2 were compared, we observed that the viscosity coefficients in the bio-composites containing 20 wt% STO nanoparticles were lower than in the polymers without STO nanoparticles. In other words, the viscous flow of the polymer chains is higher at 20 wt% STO nanoparticles. At 0 wt% STO nanoparticles, there is a reduction in the mobility of the polymer chains due to the higher viscosity.

Table 6. Burger coefficients for biocomposites made of 0 wt% STO nanoparticles.

Temperature	E_1 MPa ⁻¹	E_2 MPa ⁻¹	η_1	η_2
100°C	0.84	0.80	33,966	704

Table 7. Burger coefficients for bio-composites made of 20 wt% STO nanoparticles.

Temperature	E_1 MPa ⁻¹	E_2 MPa ⁻¹	η_1	η_2
100°C	0.51	0.50	28,704	368

In order to determine the viscosity effects on the creep deformation of the composites, we analyzed the viscosity of the solutions: 20 wt% STO and 0 wt% STO. The results suggest that the bio-composites containing 20 wt% STO nanoparticles possessed lower viscosity than the polymers without nanoparticles, as shown in Figure 32.

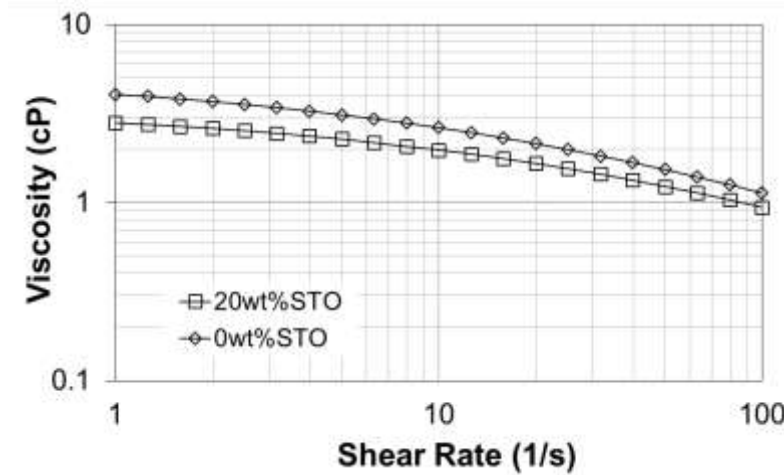


Figure 32. Viscosity study of bio-composites made of 15 v% Cel containing 0 wt% STO and 20 wt% STO nanoparticles.

Recent studies demonstrated that the addition of nanoparticles can decrease the solution viscosity, which can be regarded as an unusual behavior. Nonetheless, Tuteja et al. stated that the solution viscosity can be affected by the entanglement of the polymer chains and the interparticle half-gap [45], [46]. In order to observe a viscosity reduction, the polymer chains must be entangled. As the polymer chains are entangled, the free volume increases, and thus, the viscosity decreases. Additionally, the interparticle half-gap (h) and the radius of gyration (R_g) play an important role in the viscosity effects. When $h < R_g$, the nanoparticles do not participate in the entanglement of the polymer chains; resulting in an increase of the free volume, and thus, decreasing the viscosity of the solution.

As stated initially, we also studied the creep strain at 25°C. At this temperature, the Burger's model fail to predict the creep behavior of the composites. It is important to underscore that the viscoelastic behavior is only observed at higher temperatures when the mobility of the polymer chains is duly affected by temperature. At 25°C, the elastic behavior predominates than the viscous behavior.

5.4 Electrical Properties

An important part of this research consisted of the assessment of electrical properties of the bio-ferroelectric nanocomposites made of chitosan, cellulose and strontium titanate nanoparticles (STO), namely the capacitance, the dielectric constant, the current density and the resistivity. For the electrical measurements, the concentration of chitosan and cellulose was set at 1.5 v% and 0.5 v%, respectively. Additionally, the percentage of particles were 10 wt% and 20 wt%. In chapter 4, we concluded that the mechanical and thermal properties lowered as the concentration of cellulose increased. As a result, we only assessed the effect of 0.5 v% of cellulose. Additionally, since the electrical properties depend on the distance between the plates and the dimensions of the capacitor, these parameters were carefully controlled. One should consider two factors: a) as the gap between the plates decreases, the capacitance of the dielectric material increases, raising also the dielectric constant, and b) the capacitance raises as the area of the plates increases.

5.4.1 Capacitance and Dielectric Constant Measurements

The results in Figure 33 suggest that the amount of cellulose lowered the capacitance of the chitosan-cellulose and polymer-STO nanoparticles composites. As presented before, this capacitance was utilized to determine the dielectric constant. According to the capacitance equation for a parallel plate capacitor (equation 7), the dielectric constant is directly proportional to the capacitance. As a result, the dielectric constant also decreased as the amount of cellulose increased. Additionally, STO nanoparticles increased the dielectric constant of the composite material, as shown in Figure 34.

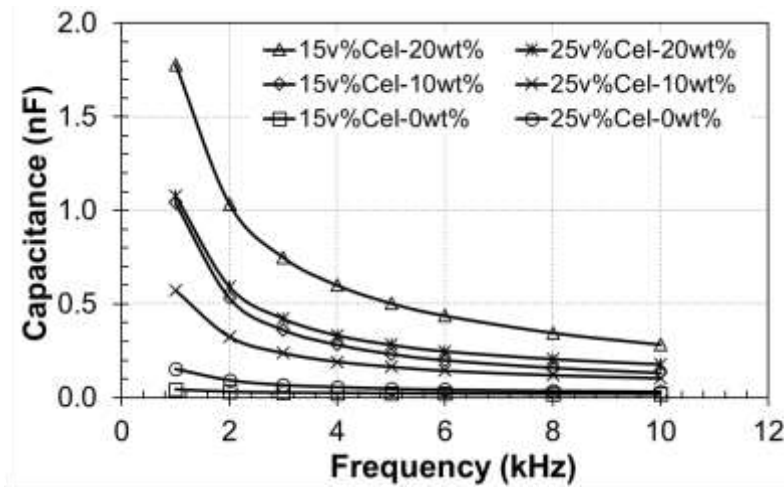


Figure 33. Capacitance as a function of frequency at an electric field of 1V.

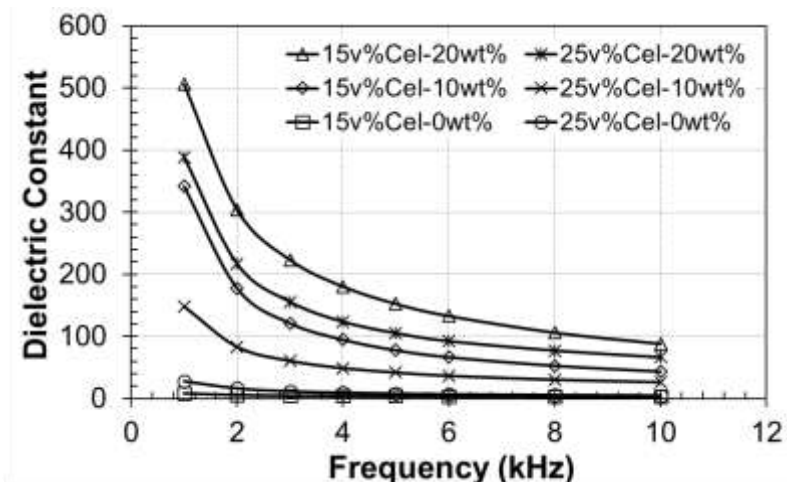


Figure 34. Dielectric constants as a function of frequency at an electric field of 1V.

At this point one should note that the electrical field frequency alters the orientation of the dipoles of the ferroelectric nanoparticles. When the ferroelectric particles are aligned with the applied electrical field, the material becomes polarized. All four polarization mechanisms will contribute to the electrical properties at a given frequency [5], [13]. At higher frequencies than the necessary for each mechanism, the dipoles cannot remain aligned to the electrical field. As a result, the polarization mechanism cannot contribute to the dielectric properties, which explains the capacitance decrease as the frequency increases.

The water content depends on the degree of the chitosan dissolution in a water/acetic acid medium and the addition of cellulose. As aforementioned, chitosan was dissolved in a water/acetic acid solution, increasing the presence of water molecules in the resulting nanocomposites. Furthermore, the interaction between the cellulose hydroxyl groups with the water molecules contributes to the larger presence of water molecules in the polymeric matrix by two means: a) linked to the (-OH) groups, or b) confined between the polymer chains due to the intermolecular hydrogen bonds [33], [34]. Related to these

interactions, Mazeau et al. stated that cellulose is a hydrophilic polymer in which the polar groups of the cellulose interacted with the water molecules of the chitosan solution, becoming retained in the polymer chains [34]. At higher electrical fields, the water content raised the space charges, which heightened the current flow through the dielectric material [37].

Additionally, higher percentages of nanoparticles increased the capacitance and the dielectric constant of the material, as presented previously. The ferroelectric nanoparticles utilized increased the stored energy in the dielectric material, enhancing the capacitance, dielectric constant and resistivity [37]. It is important to recall that the nanoparticles dispersion affects the electrical properties of the bio-composites. In order to enhance this dispersion, it is recommended to reduce the particle size to the nanoscale as Barber et al. did in their study of particle size effects on electrical properties [37]. Nanoparticles become better dispersed, increasing the surface area of the nanoparticles in the organic layer. As a result, the properties of polymer-particles interface become dominant over the bulk properties of the constituents, raising the dielectric constant.

5.4.2 Current Density and Resistivity Measurements

According to our results, higher current density was recorded as the voltage increased (Figure 35). In effect, as a result of the water content in the nanocomposite, higher percentages of cellulose increased the current passing through the capacitor. Moreover, the percentage of STO nanoparticles greatly affects the electrical properties of the nanocomposites. It has been proven, therefore, that the STO nanoparticles did improve the ability of the capacitor to store more energy; decreasing the current flow through the capacitor.

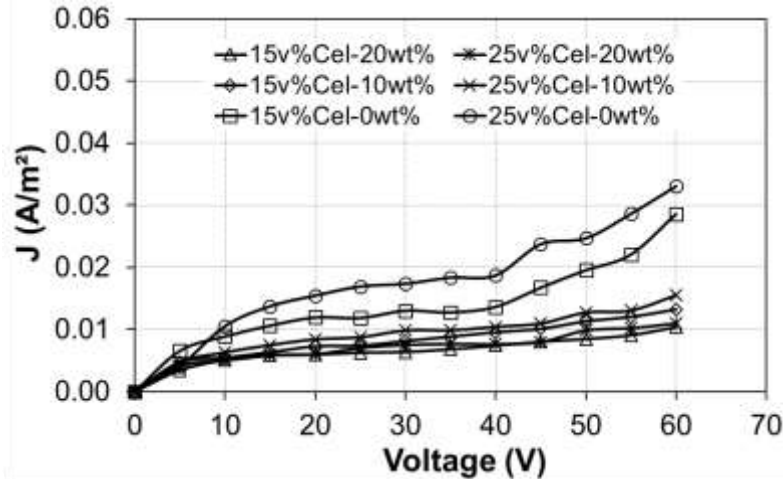


Figure 35. Current density as a function of voltage for bio-ferroelectric nanocomposites.

In order to determine the conductivity divided by the capacitor thickness (σ_t), i.e. the conductivity per unit thickness, we applied a linear regression analysis to the curves of current density as a function of the electric field (V). The linear regression provides the slope of the curve, which represents σ_t of the dielectric material. After that, the resistivity per unit thickness (ρ_t) was obtained as the inverse of the conductivity per unit thickness. According to these results, the resistivity per unit thickness of the dielectric material increased for higher amounts of STO nanoparticles while the addition of cellulose lowered it (Figure 36). Cellulose increased the water content in the polymeric matrix, reducing the resistivity of composites. Conversely, the addition of STO nanoparticles increased the stored energy of the capacitor, which raised the resistivity of the dielectric material.

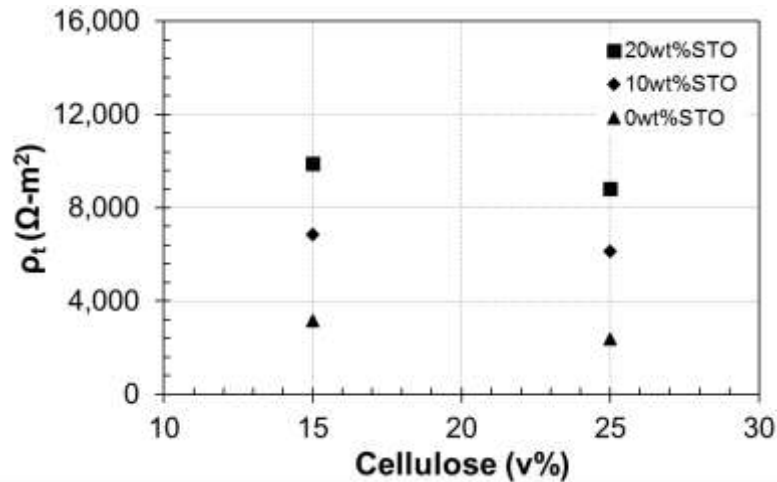


Figure 36. Resistivity as a function of cellulose percent of the bio-ferroelectric nanocomposites.

5.4.3 Electrical Measurements of Chitosan-Cellulose-STO nanoparticles and Commercial Ceramic Capacitors

As a baseline and for the sake of comparison, the electrical properties of the polymer-STO nanocomposites and four types of commercial ceramic-disk capacitors (capacitance, 0.001 μF) were measured under similar conditions. As shown in Figure 37, the capacitance of the polymer-STO nanocomposite dramatically decreased as the voltage increased while the capacitance remained constant in the commercial capacitors from 5V to 60V.

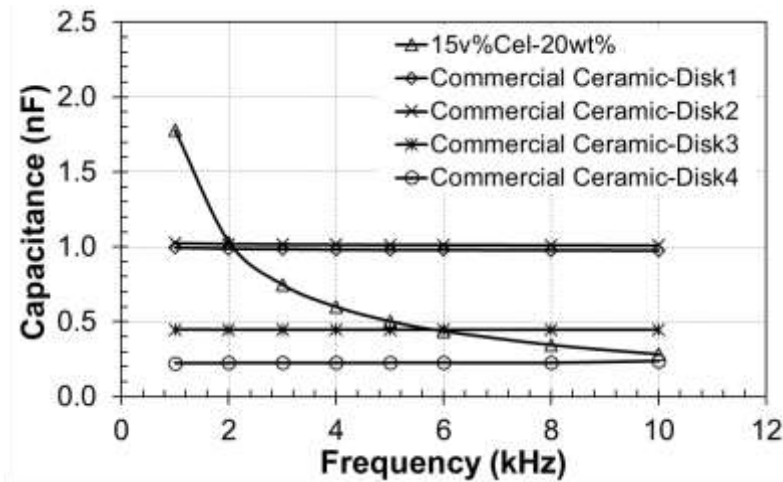


Figure 37. Capacitance measurements for the polymer / STO nanocomposite and four commercial ceramic-disk capacitors.

The capacitance behaves differently as a function of the applied frequency due to the nature of each dielectric material. For polymer-STO nanocomposites, the presence of water molecules generated space charge when an electrical field is applied. These space charges are highly polarized at lower frequencies. For ceramic capacitors, the electric field generates covalent polarization, which alters the dimensions of the crystalline structure [5], [26].

Capacitors made of particles-polymer composites and those made of ceramics exhibited different nonlinear dielectric properties, as shown in Figure 37. This adjustable quality is commonly known as tunability, which is extremely interesting for applications in microwave tunable circuits and flexible electronics. For example, to improve future microwave networks it is required to have high-performance tunable elements such as capacitors. As a result, researchers are interested in the fabrication of flexible organic electronics for a cost effective perspective and environment friendly point of view such as chitosan-based composites [13], [47].

Furthermore, the current flow was also studied for all said dielectric materials, i.e. polymer-STO nanocomposite and commercial ceramic capacitors. As shown in Figure 38, the current flow raised as the applied voltage increased for all materials. However, the results showed higher current flow through the commercial ceramic capacitors than through the polymer-STO nanocomposite. Figure 38-b demonstrates that the increasing current flow in this latter material only varies between 0 and $12 \cdot 10^{-4}$ mA for the same voltage range. For commercial ceramic disk capacitors, the maximum current flow was 1.0 mA while $1.0 \mu\text{A}$ was measured for the polymer-STO nanocomposite at 60 V.

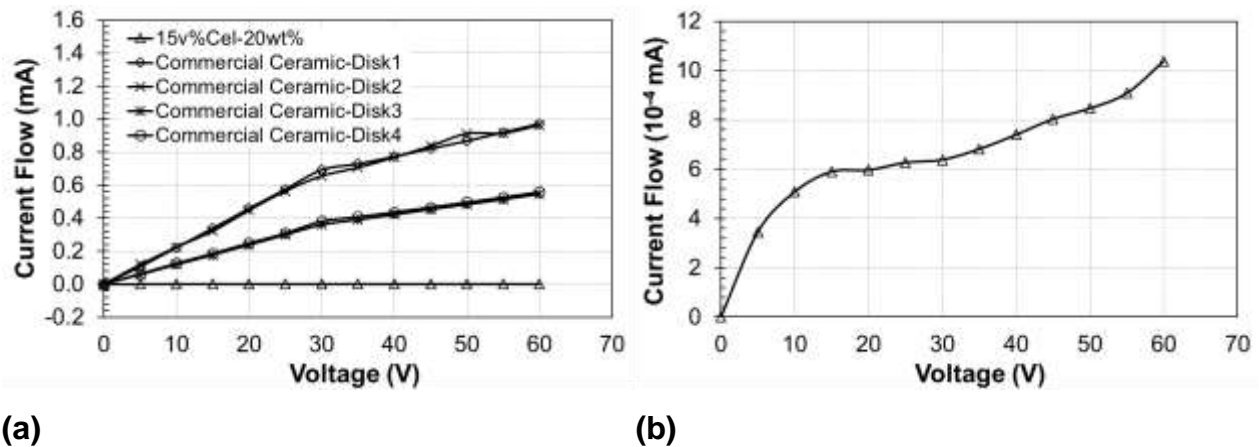


Figure 38. Current flow at different voltages: (a) commercial capacitors and experimental one; (b) detail of the polymer-STO nanocomposite response.

5.5 Degradation Analysis

The absorbed mass by the polymer-STO nanoparticles composites for 5 hours is shown in Figure 39, 40 and 41 for different aqueous media. The results showed that the addition of cellulose and nanoparticles delayed the degradation of the polymeric films due to the lower water content retained into the polymeric films. An interesting behavior was observed at 0.33 hour in which high absorbed mass was registered. After this time, the

absorbed mass diminished to eventually slightly increase with time. Moreover, the degradation of the composites was affected by the solution: hydrochloric acid, acetic acid and water. For hydrochloric acid, the absorbed mass ranged between 0.02 g to 0.45 g since 0.02 g to 0.23 g for acetic acid and 0.04 g to 0.18 g for water.

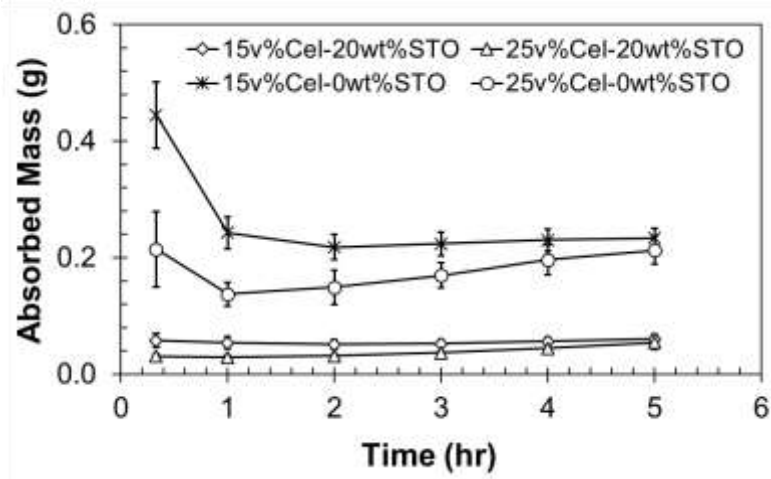


Figure 39. Absorbed mass as a function of time for bio-composites made of chitosan, cellulose and STO nanoparticles degraded in hydrochloric acid solution, pH 3.3.

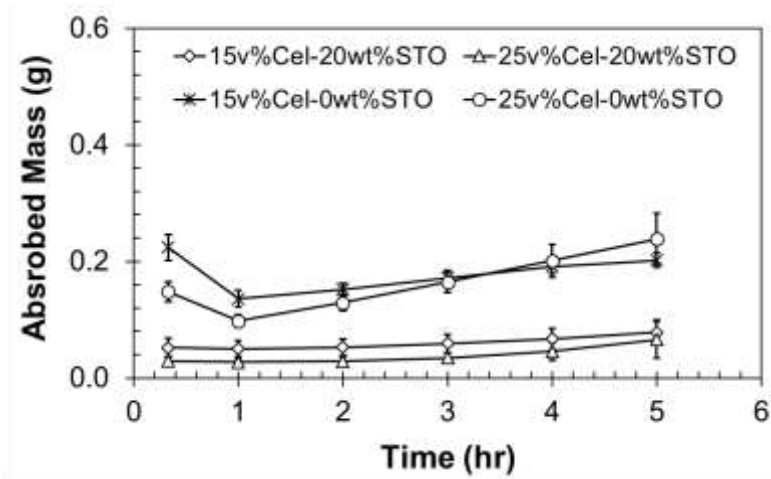


Figure 40. Absorbed mass as a function of time for bio-composites made of chitosan, cellulose and STO nanoparticles degraded in acetic acid solution, pH 4.1.

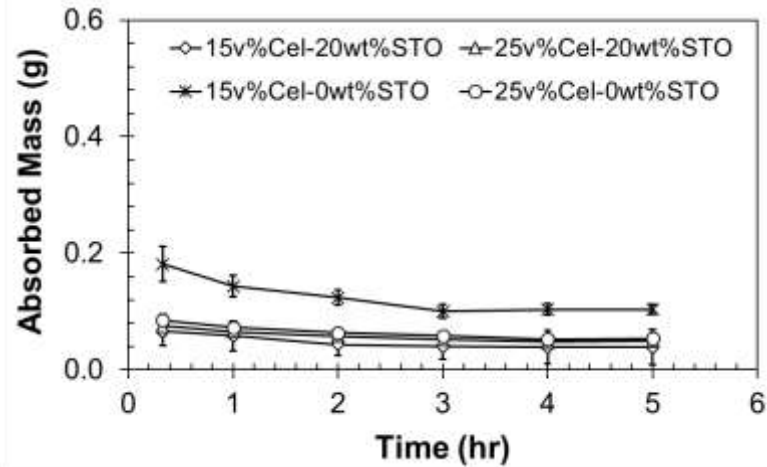


Figure 41. Absorbed mass as a function of time for bio-composites made of chitosan, cellulose and STO nanoparticles degraded in water, pH 6.0.

As presented, we attempted to degrade the bio-composites in different aqueous solutions: hydrochloric acid, acetic acid and water. We found that the bio-composites highly degraded in a hydrochloric acid solution than in acetic acid solution and in water. An interesting aspect of all these solutions is the pH values: hydrochloric acid (pH 3.3), acetic acid (pH 4.1) and water (pH 6.0). The pH value of the deionized water was not 7.0 due to the removal of the minerals.

The marked differences between the results in HCl solution and acetic acid solution requires further explanation. The literature classifies HCl as a strong acid and acetic acid as a weak one. This classification let us understand the dissociation of the acids in an aqueous solution. The strong acids completely dissociate in its ions while, conversely, the weak acids partially dissociate. Thus, the complete dissociation of the strong acids can raise the protonation of the amine groups.

As stated in previously studies, the amine groups in the chitosan structure are protonated at pH values below 6.0; protonation means that the hydrogen protons (H^+) adhered to the amine groups ($-NH_2$), forming (NH_3^+) groups [7], [35], [36]. These groups (NH_3^+) raise the

negative charges, increasing the electrostatic repulsions between the polymeric chains, which led the relocation of water molecules between the chains, as shown in Figure 32 [48]. These electrostatic repulsions increase the swelling of the bio-composites.

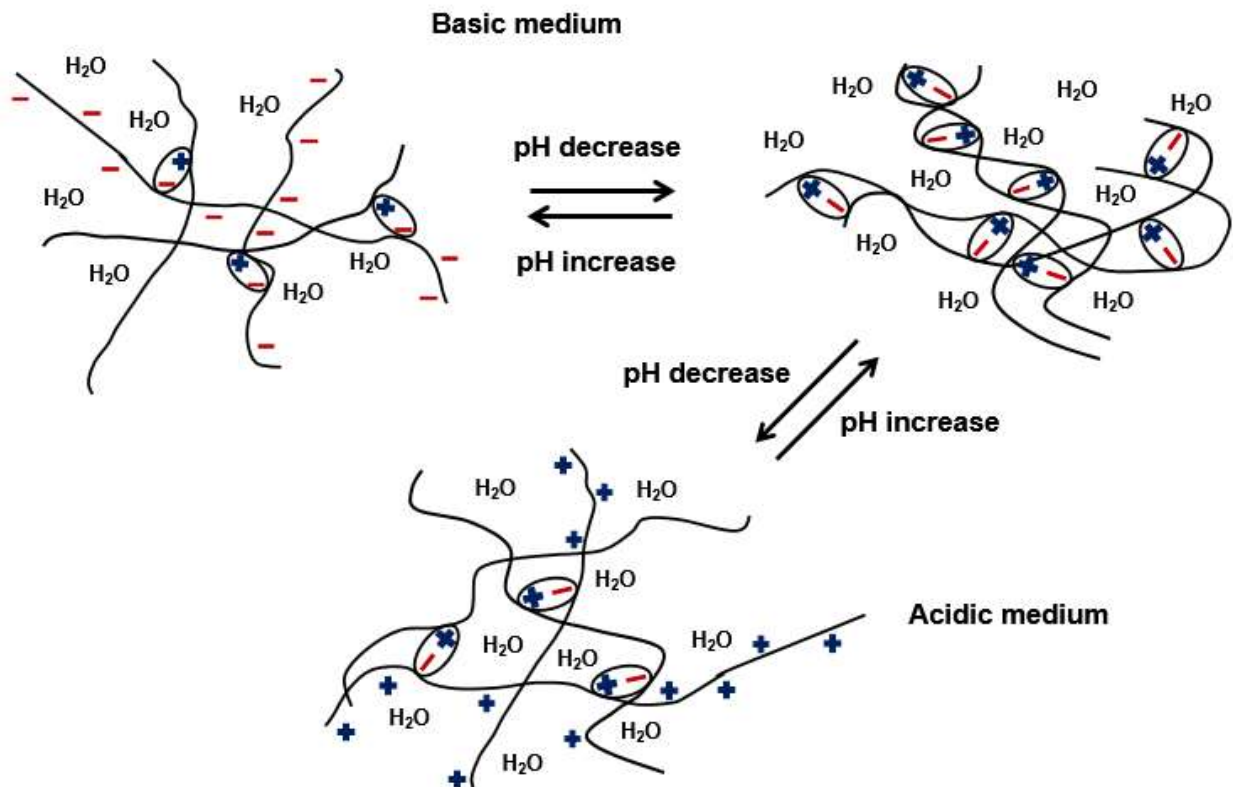


Figure 42. Polymer chains under different pH values: (a) pH 7.0; (b) pH 4.0 [48].

As mentioned before, the results showed a maximum absorbed mass at 0.33 hours. As seen before, the absorbed mass decreased and then after 1 hour slightly increased. We believe that these behavior is due to the pH neutralization of the solution. Initially, the polymer absorbed a great amount of water because most of the (-NH_2) groups are protonated, rendering the formation of (NH_3^+) groups [7], [35]. Seemingly this reaction reached the maximum protonation at 0.33 hours, eventually decreasing due to the

changes of the pH values from the acid level (pH ~ 3.0) to the basic level (pH ~ 6.0). As a result, the swelling of the bio-composites decreases. This is considered as a reversible reaction and dramatically affected by the pH of the solution.

After this study, we measured the percentage of dry mass after the degradation analysis, as shown in Figure 43. As expected, the addition of cellulose and STO nanoparticles lowered the composites degradation. When the effects of hydrochloric and acetic acids were compared, the results indicated that the polymer degraded more in hydrochloric acid than in acetic acid.

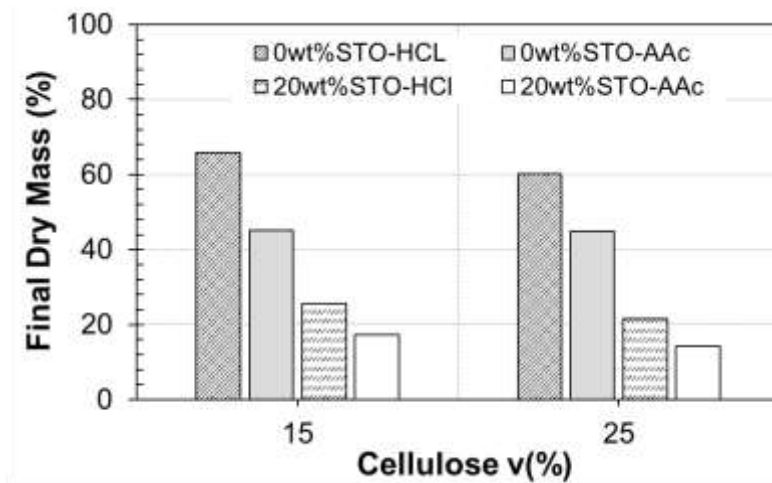


Figure 43. Dry mass for bio-composites made of chitosan, cellulose and STO nanoparticles.

Afterwards, the dissolution rate constant (k_{dis}) was obtained using equation 22. The results are presented in Figure 44 [49].

$$M_{pt} = M_{p0} - k_{dis} A_t t \quad (22)$$

M_{pt} is the dry mass at time t , M_{p0} is the dry mass at time $t = 0$, A_t is the surface area of the specimen at time t . The dissolution rate constant (k_{dis}) decreased for higher amounts of cellulose and STO nanoparticles. Once again, hydrochloric acid highly degraded the nanocomposites.

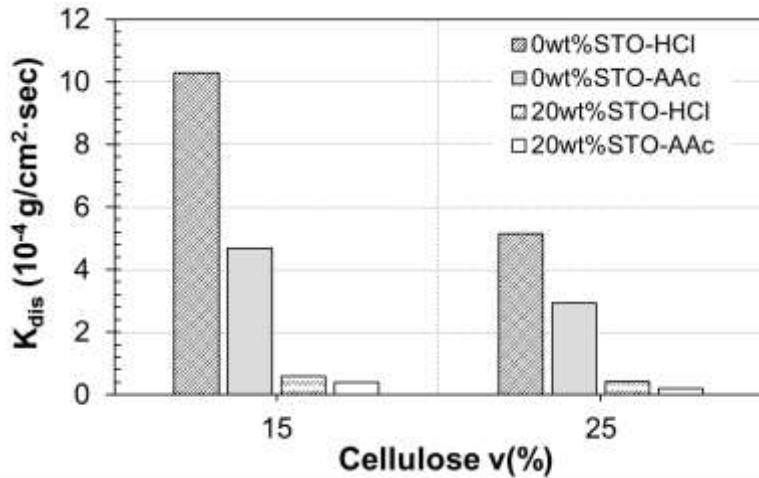


Figure 44. Dissolution rate constant (k_{dis}) for bio-composites made of chitosan, cellulose and STO nanoparticles.

Figure 45 and 46, shows the FT-IR spectra of bio-composites made of 25 v% of cellulose degraded in both acid solutions. In the spectra obtained for the composites without degradation, one can observed bands at 3400 cm^{-1} characteristic of ($-\text{OH}$) groups as well as two bands at 1650 cm^{-1} and 1560 cm^{-1} , which represent the amide I and ($-\text{NH}_2$), respectively [35]. Moreover, these spectra show a band near 1733 cm^{-1} characteristic of ($-\text{CHO}$) of cellulose [35].

Figure 45 and 46 reveal that the degradation is readily detected in the FTIR spectra that show real bands and negative bands, which can change their shape and position according to Davidson [50]. For the degraded polymers, the characteristics bands of chitosan and cellulose disappeared. However, the spectrum reveals a band near 1072

cm⁻¹ characteristic of (C–O) groups, which are in the chitosan and cellulose structure. Furthermore, the results suggest that the addition of the STO nanoparticles reduced the degradation of the bio-composites.

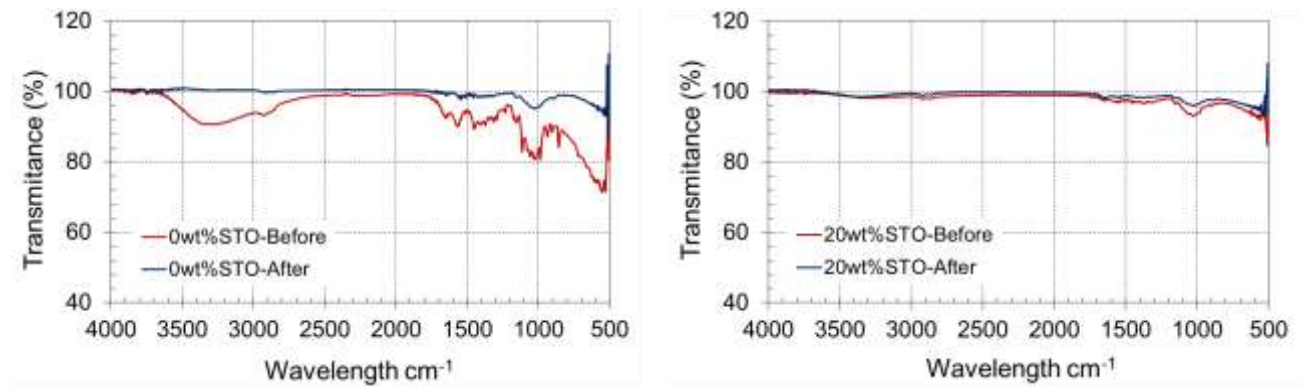


Figure 45. Fourier transform infrared spectra for bio-composites made of 25 v% of cellulose in acetic acid solution.

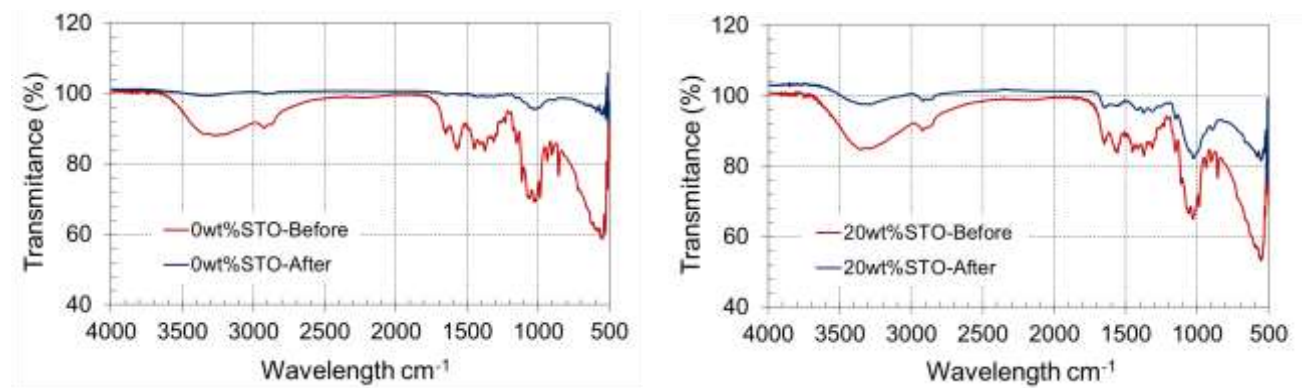


Figure 46. Fourier transform infrared spectra for bio-composites made of 25 v% of cellulose in hydrochloric acid solution.

In addition, the ultimate tensile strength was obtained for bio-composites degraded in a hydrochloric acid. As shown in Figure 47 and 48, the UTS diminished after the degradation process. For 0 wt% of STO nanoparticles, the UTS decreased 13 MPa for 15 v% of cellulose and 7.5 MPa for 25 v% of cellulose. Additionally, a reduction of 6 MPa was observed for the bio-composites containing 20 wt% of STO nanoparticles. It is

evident that the degradation process lowered the mechanical resistance of the bio-composites. When the polymers are degraded, the integrity of the materials structure is compromised with the loss of mass and scission of chains.

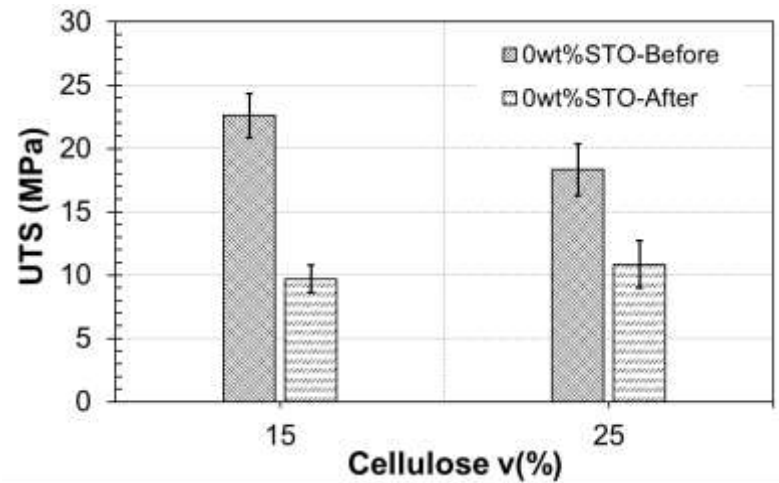


Figure 47. Tensile analysis for degraded bio-composites made of 15 v% and 25 v% of cellulose in hydrochloric acid solution.

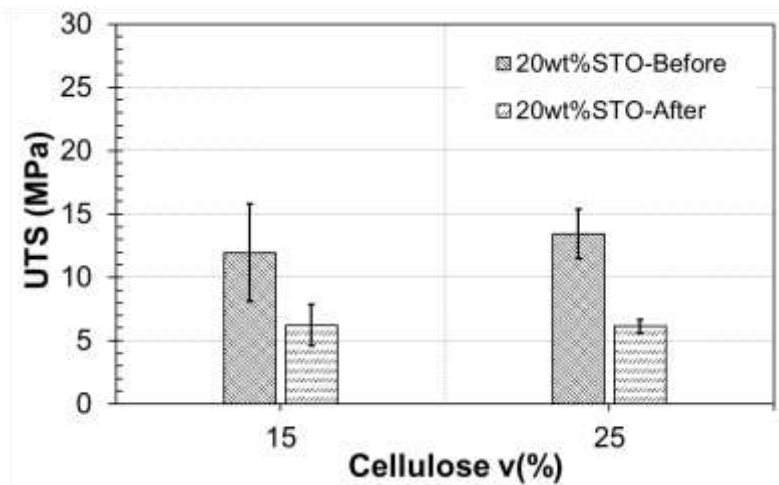


Figure 48. Tensile analysis for degraded bio-composites made of 15 v% and 25 v% of cellulose in hydrochloric acid solution.

After the degradation analysis on different acidic solutions, we concluded that higher degradation was observed for strong acids (HCl) than weak acids (acetic acids). Furthermore, we found that the degradation is affected by the pH of the solution. Even though the composites degraded on acidic solutions, the addition of STO nanoparticles delayed it.

We decided to study the degradation of the composites because capacitors can be exposed to acidic conditions due to the breakdown of another electrical component. There are components based on a liquid or gel containing high concentration of ions, namely as electrolytic capacitors. These capacitors achieved larger capacitance than others capacitors, but they present several drawbacks; including large leakage currents, overheating and limited lifetime. When this capacitors failed, they can cause damage to other components in the electrical circuit. As a result, we decided to study the degradation of the composites in order to observe its behavior under some acidic conditions.

The degradation analysis help us to predict the degradation of the composites under different aqueous media. In our analysis, we utilized higher concentrations than the utilized in the fabrication of the electrical components. However, we expect that the degradation of the composites behaves similar to the presented at higher concentrations. It is known that at lower concentrations, the composites degraded slowly.

6 CONCLUSIONS

This research aimed to study the mechanical, thermal and electrical properties of composites made of chitosan, cellulose and strontium titanate nanoparticles (STO). The variables considered includes: concentration of cellulose (0.5 v% and 1.0 v%), the volume percentages of cellulose (5 v%, 15 v% and 25 v%) added into each small solution, the acetic acid concentration (1.25 v% and 2.50 v%) utilized for the chitosan dissolution and the amounts of STO nanoparticles, 10 wt% and 20 wt%.

The chitosan-cellulose and polymer-STO nanoparticles composites were successfully fabricated via sol gel casting method in which the cellulose did not precipitated. Strontium titanate were dispersed in the polymeric matrix. To achieve better dispersion of the nanoparticles, the particles size was reduced from 43 nm to 18 nm using the high ball mill technique, which also reduced the agglomerates of the nanoparticles. As stated in the analysis, this particles tend to agglomerate due to the high electrostatic forces between each particles. We achieved a high dispersion of the nanoparticles in the polymeric matrix.

Mechanical and thermal analysis allowed establishing that the addition of cellulose can adversely affect the ultimate tensile strength and the degradation temperature of the composites made of chitosan and cellulose. Higher amounts of cellulose increased the water content in the polymeric films due to its hydrophilic behavior. For composites containing strontium titanate nanoparticles, the ultimate tensile strength and the degradation temperature slightly raised as the amount of cellulose increased. In this composites, cellulose and the nanoparticles increased the pH of the solution from 3.42 to

5.10, reducing the electrostatic forces between the chains, and thus, the water content decreased.

Even though, the nanoparticles slightly increased the ultimate tensile strength and the degradation temperature of the composites, higher amounts of nanoparticles lowered those properties. We attributed such reduction to the detrimental effect on the interfacial energy between polymer-nanoparticles. Higher percentages of nanoparticles can increase the interfacial energy between polymer-nanoparticles, probably generating cracks through the nanoparticles, which then propagate through the polymeric film.

In addition, the effects of the acetic acid concentration were analyzed. At higher concentrations of acetic acid, the ultimate tensile strength and the degradation temperature of the composites without nanoparticles decreased. As mentioned before, at lower pH values ($\text{pH} < 6.0$), the amine groups are highly protonated, increasing the electrostatic repulsions between the polymer chains. As a result, the polymer chains separate from each other, resulting in the relocation of more water molecules between the chains.

Furthermore, the creep studies of the chitosan-cellulose and polymer-STO nanoparticles composites under an applied load of 1.0N at 25°C and 100°C revealed that the creep compliance of each composite was greater at 100°C. Additionally, the STO nanoparticles raised the creep compliance of the bio-ferroelectric composites compared to the chitosan-cellulose composites. Higher percentages of chitosan increase the brittleness of the composites due to its high stiffness and resistance to deformation. It is believed that the nanoparticles agglomeration could have affected the interface between the nanoparticles and the polymeric matrix. These agglomerates could slip at higher shear stresses,

resulting in the formation of new cracks that propagate through the polymeric matrix at slow velocity.

Viscosity can affect the creep deformation of the composites, i.e. high viscosity reduces the creep deformation of the composites, as observed in the biopolymers without STO nanoparticles. The addition of the nanoparticles reduce the viscosity of the solution, which can be attributed to their interaction with the polymer chains. In this case, the nanoparticles did not participate in the entanglement of the polymer chains, reducing the viscosity of the solution.

In terms of the measured electrical properties, the addition of the STO nanoparticles raised the dielectric constant, capacitance, and electrical resistivity of the composites. Similarly, the addition of the nanoparticles decreased the composites current density. At a maximum of 60V of applied voltage the dielectric rupture for the bio-ferroelectric nanocomposites did not occur.

In order to study the degradation of the composites, the effects of different aqueous solutions were analyzed: hydrochloric acid (pH 3.3), acetic acid (pH 4.1) and water. The results showed that the composites degraded more in the HCl solution than in the acetic acid one. Through FT-IR analyses, the degradation of the composites was observed; the spectra rendered a reduction of all the characteristics peaks of chitosan and cellulose. In addition, the ultimate tensile strength for composites treated with hydrochloric acid was lower than composites treated with acetic acid and water (pH 6.0). At lower pH values, the protonation of the amine groups ($-NH_2$) takes place, resulting in the formation of (NH_3^+) groups. These ammonium groups raise the negative charges, increasing the electrostatic repulsions between the polymer chains. Higher electrostatic repulsions led

the relocation of more water molecules between the polymer chains, increasing the water content in the polymer; hence, the polymer degradation increases.

7 REFERENCES

- [1] E. Dujarding and S. Mann, "Bio-inspired Materials Chemistry **," *Adv. Mater.*, vol. 14, no. 11, pp. 1–14, 2002.
- [2] S. K. Shukla, A. K. Mishra, O. A. Arotiba, and B. B. Mamba, "Chitosan-Based Nanomaterials: A State-of-the-Art Review," *Int. J. Biol. Macromol.*, vol. 59, pp. 46–58, 2013.
- [3] B. A. Cheba, "Chitin and Chitosan : Marine Biopolymers with Unique Properties and Versatile Applications," *J. Biotechnol. Biochem.*, vol. 6, no. 3, pp. 149–153, 2011.
- [4] D. R. Kingery, W.D., Bowen, H.K. and Uhlmann, *Introduction to Ceramics*, Second Edi. 1976, pp. 913–974.
- [5] B. Carter and G. Norton, *Ceramic Materials: Science and Engineering*, Second Edi., vol. 56, no. 5. 2001, pp. 573–576.
- [6] G. H. Haertling, "Ferroelectric Ceramics : History and Technology," vol. 818, 1999.
- [7] J. Hosokawa, M. Nishiyama, K. Yoshihara, T. Kubo, and A. Terabe, "Reaction between Chitosan and Cellulose on Biodegradable Composite Film Formation," *Ind. Eng. Chem. Res.*, vol. 30, no. 4, pp. 788–792, 1991.
- [8] D. Nordqvist, J. Idermark, M. S. Hedenqvist, M. Gällstedt, M. Ankerfors, and T. Lindström, "Enhancement of the wet properties of transparent chitosan-acetic-acid-salt films using microfibrillated cellulose.," *Biomacromolecules*, vol. 8, no. 8, pp. 2398–403, Aug. 2007.
- [9] N. Nemet, V. Soso, and V. Lazic, "Effect of Glycerol Content and pH Value of Film-Forming Solution on the Functional Properties of Protein-Based Edible Films," *APTEFF*, vol. 41, pp. 57–67, 2010.
- [10] L. H. Cheng, A. Karim, M. H. Norziah, A. Fazilah, and C. C. Seow, "Interactive Effects of Water-Glycerol and Water-Sorbitol on Physical Properties of Konjac Glucomannan Films," *Food Res. Int.*, pp. 1–26.
- [11] Y. P. Chang, A. Karim, and C. C. Seow, "Interactive Plasticizing-Antiplasticizing Effects of Water and Glycerol on the Tensile Properties of Tapioca Starch Films," *Food Hydrocoll.*, vol. 20, pp. 1–8, 2006.
- [12] S. D. Jang, J. H. Kim, C. Zhijiang, and J. Kim, "The Effect of Chitosan Concentration on the Electrical Property of Chitosan-Blended Cellulose Electroactive Paper," *Smart Mater. Struct.*, vol. 18, p. 015003, 2008.

- [13] A. M. Neagu, L. Petronela, A. Cazacu, and L. Mitoseriu, "Impedance Analysis and Tunability of BaTiO₃-Chitosan Composites: Towards Active Dielectrics for Flexible Electronics," *Compos. Part B*, vol. 66, pp. 109–116, 2014.
- [14] V. Bansal, P. Poddar, A. Ahmad, and M. Sastry, "Room-Temperature Biosynthesis of Ferroelectric Barium Titanate Nanoparticles," *J. Am. Chem. Soc.*, vol. 128, no. 36, pp. 11958–11963, 2006.
- [15] E. P. Gorzkowski and M. J. Pan, "Dielectric Composites for Naval Applications," *J. Miner. Met. Mater. Soc.*, vol. 66, no. 2, p. 2014, 2014.
- [16] Z. Ahmad, "Polymeric Dielectric Materials," in *Dielectric Material*, 2012, pp. 3–26.
- [17] R. Duncan, "The Dawning Era of Polymer Therapeutics," *Nat. Rev. Drug Discov.*, vol. 2, pp. 347–360, 2003.
- [18] O. A. El Seoud, H. Nawaz, and E. Arêas, "Chemistry and Applications of Polysaccharide Solutions in Strong Electrolytes/Dipolar Aprotic Solvents: An Overview," *Molecules*, vol. 18, pp. 1270–1313, 2013.
- [19] M. Rinaudo, "Chitin and Chitosan: Properties and Applications," *Prog. Polym. Sci.*, vol. 31, pp. 603–632, 2006.
- [20] C. T. Andrade and E. G. A. Rojas, "Biopolymers," in *Biopolymer Engineering in Food Processing*, pp. 46–53.
- [21] M. Thongngam and J. McClements, "Characterization of Interactions between Chitosan and an Anionic Surfactant," *Agric. Food Chem.*, vol. 52, pp. 987–991, 2004.
- [22] W. Ding, Q. Lian, R. J. Samuels, and M. B. Polk, "Synthesis and Characterization of a Novel Derivative of Chitosan," *Polymer (Guildf)*, vol. 44, pp. 547–556, 2003.
- [23] C. Chen, Z. Gao, X. Qiu, and S. Hu, "Enhancement of the controlled-release properties of chitosan membranes by crosslinking with suberoyl chloride," *Molecules*, vol. 18, no. 6, pp. 7239–7252, 2013.
- [24] C. Olsson and G. Westman, "Direct Dissolution of Cellulose : Background , Means and Applications, Cellulose-Fundamental Aspects," 2013, pp. 143–178.
- [25] G. H. Haertling, "Ferroelectric Ceramics: History and Technology," *J. Am. Ceram. Soc.*, vol. 82, no. 4, pp. 797–818, 1999.
- [26] W. D. Kingery, H. K. Bowen, and D. R. Uhlmann, *Introduction to Ceramics*. 1976, pp. 913–974.

- [27] M. Golio, *The RF and Microwave Handbook*. 2008, p. Appendix A–13,14.
- [28] a. Plaseied and a. Fatemi, “Tensile Creep and Deformation Modeling of Vinyl Ester Polymer and Its Nanocomposite,” *J. Reinf. Plast. Compos.*, vol. 28, no. 14, pp. 1775–1788, 2009.
- [29] C. Olsson and G. Westman, “Direct Dissolution of Cellulose: Background, Means and Applications,” in *Cellulose–Fundamental Aspects*, 2013, pp. 143–178.
- [30] S. Hirano, T. Yogo, W. Sakamoto, K. Banno, and R. Fukuzawa, “Novel electro-rheological nanocrystalline dielectric particles modified with or embedded in organics,” *J. Eur. Ceram. Soc.*, vol. 24, no. 6, pp. 1911–1917, Jan. 2004.
- [31] A. W. Burton, K. Ong, T. Rea, and I. Y. Chan, “On the Estimation of Average Crystallite Size of Zeolites from the Scherrer Equation: A Critical Evaluation of its Application to Zeolites with One-Dimensional Pore Systems,” *Microporous Mesoporous Mater.*, vol. 117, pp. 75–90, 2009.
- [32] ASTM International, “D150-98: Standard Test Methods for AC Loss Characteristics and Permittivity (Dielectric Constant) of Solid Electrical Insulation,” vol. 10, pp. 1–20, 1999.
- [33] Z. H. Ping, Q. T. Nguyen, S. M. Chen, J. Q. Zhou, and Y. D. Ding, “States of Water in Different Hydrophilic Polymers—DSC and FTIR Studies,” *Polymer (Guildf).*, vol. 42, pp. 8461–8467, 2001.
- [34] K. Mazeau, “The Hygroscopic Power of Amorphous Cellulose: A Modeling Study,” *Carbohydr. Polym.*, vol. 117, pp. 585–591, 2015.
- [35] E. P. Azevedo, “Aldehyde-Functionalized Chitosan and Cellulose: Chitosan Composites: Application as Drug Carriers and Vascular Bypass Grafts,” University of Iowa, 2011.
- [36] S. Strnad, O. Šauperl, and L. Fras-Zemljic, “Cellulose Fibres Functionalised by Chitosan : Characterization and Application,” in *Biopolymers*, 2008, pp. 181–200.
- [37] P. Barber, S. Balasubramanian, Y. Anguchamy, S. Gong, A. Wibowo, H. Gao, H. J. Ploehn, and H.-C. Loye, *Polymer Composite and Nanocomposite Dielectric Materials for Pulse Power Energy Storage*, vol. 2. 2009, pp. 1697–1733.
- [38] V. Uvarov and I. Popov, “Metrological Characterization of X-ray Diffraction Methods for Determination of Crystallite Size in Nano-Scale Materials,” *Mater. Charact.*, vol. 58, pp. 883–891, 2007.
- [39] M. S. Jamil, I. Ahmad, and I. Abdullah, “Effects of Rice Husk Filler on the Mechanical and Thermal Properties of Liquid Natural Rubber Compatibilized High-

- Density Polyethylene/Natural Rubber Blends,” *J. Polym. Res.*, vol. 13, pp. 315–321, 2006.
- [40] M. S. Ibrahim, S. M. Sapuan, and A. A. Faieza, “Mechanical and Thermal Properties of Composites from Unsaturated Polyester Filled with Oil Palm Ash,” *J. Mech. Eng. Sci.*, vol. 2, pp. 133–147, 2012.
- [41] D. Stokke, Q. Wu, and G. Han, “Introduction to Wood and Natural Fiber Composites,” in *Wiley Series in Renewable Resources*, 2014.
- [42] Y. Dong, Y. Ruan, H. Wang, Y. Zhao, and D. Bi, “Studies on Glass Transition Temperature of Chitosan with Four Techniques,” *J. Appl. Polym. Sci.*, 2003.
- [43] S.-D. Jang, J.-H. Kim, C. Zhijiang, and J. Kim, “The Effect of Chitosan Concentration on the Electrical Property of Chitosan-Blended Cellulose Electroactive Paper,” *Smart Mater. Struct.*, vol. 18, pp. 1–5, 2009.
- [44] J.-L. Yang, Z. Zhang, A. K. Schlarb, and K. Friedrich, “On the Characterization of Tensile Creep Resistance of Polyamide 66 Nanocomposites. Part II: Modeling and Prediction of Long-Term Performance,” *Polymer (Guildf.)*, vol. 47, pp. 2791–2801, 2006.
- [45] A. Tuteja, P. M. Duxbury, and M. E. Mackay, “Multifunctional Nanocomposites with Reduced Viscosity,” *Macromolecules*, vol. 40, no. 26, pp. 9427–9434, 2007.
- [46] A. Tuteja, M. E. Mackay, and C. J. Hawker, “Effect of Ideal , Organic Nanoparticles on the Flow Properties of Linear Polymers : Non-Einstein-like Behavior,” pp. 8000–8011, 2005.
- [47] M. Zirkl, a. Haase, a. Fian, H. Schön, C. Sommer, G. Jakopic, G. Leising, B. Stadlober, I. Graz, N. Gaar, R. Schwödiauer, S. Bauer-Gogonea, and S. Bauer, “Low-Voltage Organic Thin-Film Transistors with High-k Nanocomposite Gate Dielectrics for Flexible Electronics and Optothermal Sensors,” *Adv. Mater.*, vol. 19, no. 17, pp. 2241–2245, Sep. 2007.
- [48] L. Hyung, Y. Michael, E. Yonaton, N. Hickok, E. David, and C. Russell, “Reversible Swelling of Chitosan and Quaternary Ammonium Modified Chitosan Brush Layers: Effect of pH and Counter Anion Size and Functionality,” *J. Mater. Chem.*, vol. 22, no. 37, pp. 19605–19616, 2013.
- [49] B. A. Miller-Chou and J. L. Koenig, “A Review of Polymer Dissolution,” *Prog. Polym. Sci.*, vol. 28, pp. 1223–1270, 2003.
- [50] R. Davidson, “Polymer Degradation Studies by FTIR,” in *Progress in Pacific Polymer Science 2*, 1992, pp. 101–111.